NASA CR-72349

ELECTROCHEMICAL CHARACTERIZATION OF NONAQUEOUS SYSTEMS FOR SECONDARY BATTERY APPLICATION

by

M. Shaw, O. A. Paez, A. H. Remanick

prepared for

NATIONAL AERONAUTICS AND SPACE ADMINISTRATION

CONTRACT NO. NAS 3-8509

SIXTH QUARTERLY REPORT

AUGUST - OCTOBER 1967

WHITTAKER CORPORATION
NARMCO RESEARCH & DEVELOPMENT DIVISION
3540 Aero Court
San Diego, California 92123

NOTICE

This report was prepared as an account of Government sponsored work. Neither the United States, nor the National Aeronautics and Space Administration (NASA), nor any person acting on behalf of NASA:

A.) Makes any warranty or representation, expressed or implied, with respect to the accuracy, completeness, or usefulness of the information contained in this report, or that the use of any information, apparatus, method, or process disclosed in this report may not infringe privately owned rights; or

B.) Assumes any liabilities with respect to the use of, or for damages resulting from the use of any information, apparatus, method or process disclosed in this report.

As used above, "person acting on behalf of NASA" includes any employee or contractor of NASA, or employee of such contractor, to the extent that such employee or contractor of NASA, or employee of such contractor prepares, disseminates, or provides access to, any information pursuant to his employment or contract with NASA, or his employment with such contractor.

Requests for copies of this report should be referred to

National Aeronautics and Space Administration
Scientific and Technical Information Division
Attention: USS-A
Washington, D. C. 20546

NASA CR-72349

SIXTH QUARTERLY REPORT

ELECTROCHEMICAL CHARACTERIZATION OF NONAQUEOUS SYSTEMS FOR SECONDARY BATTERY APPLICATION

August, 1967 - October, 1967

by

M. Shaw, O. A. Paez, A. H. Remanick

prepared for

NATIONAL AERONAUTICS AND SPACE ADMINISTRATION

November 17, 1967

CONTRACT NAS 3-8509

Technical Management
Space Power Systems Division
National Aeronautics and Space Administration
Lewis Research Center, Cleveland, Ohio
Mr. Robert B. King

NARMCO RESEARCH AND DEVELOPMENT DIVISION

OF

WHITTAKER CORPORATION
3540 Aero Court
San Diego, California 92123

TABLE OF CONTENTS

CYCLIC VOLTAMMOGRAMS

LIST OF TABLES

ELECTROCHEMICAL CHARACTERIZATION OF NONAQUEOUS SYSTEMS FOR SECONDARY BATTERY APPLICATION

by

M. Shaw, O. A. Paez, A. H. Remanick

ABSTRACT

Multisweep cyclic voltammograms have been obtained for an additional 161 systems comprising zinc, cadmium, molybdenum, indium, iron, vanadium, chromium, and manganese electrodes in dimethylformamide, and propylene carbonate solutions of chlorides, perchlorates, and fluorides.

Voltammograms are presented for twenty-two of these systems. Tabular data includes peak current density, sweep index, anodic-to-cathodic peak displacement, coulombic ratio, and discharge capacity. Systems exhibiting neither anodic nor cathodic peaks are listed, as well as those causing instrument overload due to a combination of high current and relatively low conductance.

SUMMARY

The electrochemical characterization of nonaqueous battery systems by nultisweep cyclic voltammetry has been continued. Cyclic voltammograms are now available on over nine hundred systems comprising silver, copper, nickel, cobalt, zinc, cadmium, molybdenum, indium, iron, vanadium, chromium, and manganese in chloride, perchlorate, and fluoride solutions of acetonitrile, butyrolactone, dimethylformamide, and propylene carbonate. Solutes consist primarily of $AlCl_3$, LiCl, $MgCl_2$, $CaCl_2$, $Mg(ClO_4)_2$, $LiClO_4$, MgF_2, $LiPF_6$, KPF_6, $Mg(PF_6)_2$, $Ca(PF_6)_2$, $LiBF_4$, $Mg(BF_4)_2$, and $Ca(BF_4)_2$. The voltammograms of twenty-two systems are included in this report.

During this reporting period cyclic voltammetry was initiated on vanadium, chromium, and manganese electrodes. In general, vanadium and chromium electrodes exhibit low or negligible cathodic electrochemical activity due possible to dissolution of the anodic product. Manganese electrodes show anodic and cathodic electrochemical activity with large peak-to-peak voltage separation.

Tables are presented listing system parameters derived from the cyclic voltammograms. These tables include data on peak current densities, sweep index, anodic-to-cathodic peak displacement, coulombic ratio, and discharge capacity. Listed also are those systems exhibiting neither anodic nor cathodic peaks, as well as those systems causing instrument overload.

INTRODUCTION

The purpose of this program is to conduct a molecular level screening by the cyclic voltammetric method on a large number of electrochemical systems in nonaqueous electrolytes, and to characterize them as to their suitability for use in high energy density secondary batteries.

Since the release and storage of energy in a battery is initiated at the molecular level of the reaction, and therefore dependent on the charge and mass transfer processes, it is essential that screening be conducted at this level, in order to eliminate those systems whose electrode processes are inadequate for secondary battery operation.

I. RESULTS

A. ANALYSIS OF CYCLIC VOLTAMMOGRAMS

Table I lists the conductivities of the solutions used in preparing the electrochemical systems screened during this quarter. The systems screened are shown in Tables II and III, representing a total of 161 systems. To date, cyclic voltammograms have been obtained for over 900 different positive-electrolyte combinations.

Curve analysis was accomplished by dividing all systems into two major groups:

1. Systems involving chloride and perchlorate electrolytes.
2. Systems involving fluoride electrolytes.

Each main group was then subdivided according to the identity of the working electrode. Each of these subgroups was further broken down according to the identity of the solvent portion of the solution. The cyclic voltammograms are then discussed in terms of the total solution. This classification facilitates data analysis, and has permitted a more significant correlation among the electrochemical systems.

Except in those cases where the metal is converted to a cathodic material prior to assembly in the measuring cell, the working electrode is the base metal itself. During the voltage sweep, the metal is oxidized to some anodic product which serves as the cathode subsequently reduced during the cathodic portion of the sweep. Each sweep cycle thus corresponds to a charge-discharge cycle. In the absence of complicating factors, it is assumed that chloride cathodes would be formed in chloride electrolytes, and fluoride cathodes in fluoride electrolytes.

Each cyclic voltammogram is identified by a CV number and labelled according to the electrochemical system, sweep rate, temperature, and zero reference representing the open circuit voltage (ocv) of the working electrode with respect to the indicated reference electrode. The current axis is in units of ma/cm^2, each unit being of variable scale depending on the X-Y recorder sensitivity setting. A maximum sensitivity of 0.1 $ma/cm^2/cm$ division has been established to avoid exaggerating the current background of poor systems. The sweep is always in a clockwise direction, the potential becoming more positive to the right. Positive currents represent anodic (charge) reactions, and negative currents represent cathodic (discharge) reactions. The voltage axis units are relative to the ocv so that voltage units are in terms of electrode polarization.

For comparative purposes, current density magnitude is classified according to very high (more than 300 ma/cm^2), high (100-300 ma/cm^2), medium high (50-100 ma/cm^2), medium low (10-50 ma/cm^2), low (1-10 ma/cm^2), and very low (less than 1 ma/cm^2).

Analysis is based on the cyclic voltammograms obtained at the lowest sweep rate, 40 mv/sec, except where additional information is required from the higher sweep rate curves to aid in the analysis.

TABLE I

ELECTROLYTE CONDUCTIVITY *

Electrolyte	Molality m	Conductivity $ohm^{-1} cm^{-1}$
Dimethylformamide-KPF_6	0.75	2.1×10^{-2}
Dimethylformamide-$Mg(ClO_4)_2$	0.75	1.9×10^{-2}
Dimethylformamide-$LiClO_4$	0.5	1.8×10^{-2}
Dimethylformamide-$LiPF_6$	0.5	9.9×10^{-3}
Dimethylformamide-$AlCl_3$ + LiCl	(1)	7.8×10^{-3}
Dimethylformamide-LiCl	0.5	7.7×10^{-3}
Dimethylformamide-$LiBF_4$	0.5	7.3×10^{-3}
Propylene carbonate-KPF_6	1.0	7.0×10^{-3}
Propylene carbonate-$LiPF_6$	0.5	5.8×10^{-3}
Propylene carbonate-$LiClO_4$	1.0	5.8×10^{-3}
Dimethylformamide-$Ca(PF_6)_2$	$<$0.5 (s)	5.8×10^{-3}
Propylene carbonate-$LiClO_4$ + $AlCl_3$	0.5 (2)	5.6×10^{-3}
Propylene carbonate-$AlCl_3$ + LiCl	(3)	5.3×10^{-3}
Propylene carbonate-$CaCl_2$	$<$0.5 (s)	5.3×10^{-3}
Propylene carbonate-$LiBF_4$	0.5	2.9×10^{-3}
Dimethylformamide-$Mg(PF_6)_2$	$<$0.5 (s)	2.8×10^{-3}
Propylene carbonate-$Ca(PF_6)_2$	$<$0.5 (s)	2.8×10^{-3}
Propylene carbonate-$Ca(PF_6)_2$	$<$0.25 (s)	2.8×10^{-3}

* In order of decreasing conductivity
(s) Saturated
(1) 0.5 m LiCl, saturated at less than 0.25 m $AlCl_3$
(2) Concentration with respect to each salt
(3) 0.5 m $AlCl_3$, saturated at less than 0.10 m LiCl

TABLE I (Cont'd.) *

Electrolyte	Molality m	Conductivity $ohm^{-1} cm^{-1}$
Dimethylformamide-$Mg(BF_4)_2$	$<$0.5 (s)	2.4×10^{-3}
Propylene carbonate-$Mg(PF_6)_2$	$<$0.25 (s)	2.4×10^{-3}
Dimethylformamide-PF_5	0.25	2.2×10^{-3}
Propylene carbonate-$MgCl_2$	$<$0.25	2.0×10^{-3}
Dimethylformamide-$Ca(BF_4)_2$	$<$0.5 (s)	1.9×10^{-3}
Propylene carbonate-$LiCl + LiClO_4$	(4)	1.3×10^{-3}
Propylene carbonate-PF_5	0.5	1.3×10^{-3}
Propylene carbonate-$Ca(BF_4)_2$	$<$0.25 (s)	8.2×10^{-4}
Propylene carbonate-$Mg(PF_6)_2$	$<$0.25 (s)	7.3×10^{-4}
Dimethylformamide-BF_3	0.5	7.0×10^{-4}
Propylene carbonate-$CaCl_2$	$<$0.10 (s)	6.9×10^{-4}

* In order of decreasing conductivity
(s) Saturated
(4) 0.05 m in $LiClO_4$, saturated with LiCl

TABLE II

ELECTROCHEMICAL SYSTEMS SCREENED
CHLORIDE AND PERCHLORATE ELECTROLYTES

Solute \ Solvent	Dimethylformamide	Propylene carbonate
$LiCl$	V, Cr, Mn	
$LiClO_4$	V, Cr, Mn	V, Cr, Mn
$LiCl + LiClO_4$		Zn, Cd, Mo, In, Fe, V
$LiClO_4 + AlCl_3$		Zn, Cd, Mo, In, Fe, V
$MgCl_2$		Mo, In, Fe
$Mg(ClO_4)_2$	V, Cr, Mn	
$CaCl_2$	Zn, Cd, Mo, In, Fe, V	Zn, Cd, Mo, In, Fe, V
$AlCl_3 + LiCl$	In, V, Cr, Mn	Mo, In, Fe, V, Cr, Mn

TABLE III

ELECTROCHEMICAL SYSTEMS SCREENED
FLUORIDE ELECTROLYTES

Solute \ Solvent	Dimethylformamide	Propylene carbonate
$LiPF_6$	Mo, In, Fe, V, Cr, Mn	Mo, In, Fe, V
KPF_6	V, Cr, Mn	V, Cr, Mn
$Mg(PF_6)_2$	Zn, Cd, Mo, In, Fe, V	Zn, Cd, Mo, In, Fe, V
$Ca(PF_6)_2$	Zn, Cd, Mo, In, Fe, V, Cr, Mn	Zn, Cd, Mo, In, Fe, V, Cr, Mn
PF_5	Zn, Cd, Mo, In, Fe, V, Cr, Mn	Zn, Cd, Mo, In, Fe, V, Cr, Mn
$LiBF_4$	Zn, Cd, Mo, In, Fe, V, Cr, Mn	Zn, Cd, Mo, In, Fe, V
$Mg(BF_4)_2$	Zn, Cd, Mo, In, Fe, V, Cr, Mn	Zn, Cd, Mo, In, Fe, V
$Ca(BF_4)_2$	Zn, Cd, Mo, In, Fe, V, Cr, Mn	Zn, Cd, Mo, In, Fe, V, Cr, Mn
BF_3	Zn, Cd, Mo, In Fe, V, Cr, Mn	

1. Systems Involving Chloride and Perchlorate Electrolytes

a. Zinc Electrode

(1) Dimethylformamide solution

Zinc in $CaCl_2$ solution results in voltage overload on the anodic sweep. The overload results from the high current and low conductivity of this system.

(2) Propylene carbonate solutions

The cyclic voltammogram for zinc in LiCl + $LiClO_4$ solution shows low anodic and cathodic currents, but no well-defined peaks. Excessive concentration polarization is indicated.

The cyclic voltammogram for zinc in $LiClO_4$ + $AlCl_3$ solution shows a single anodic peak and no cathodic peak within the 2 volt scan. Expansion of the sweep range shows a cathodic peak at more negative potentials. Large peak-to-peak voltage separations have occurred for zinc with $LiClO_4$ alone in propylene carbonate (Ref. 1, Fig. 16), similar to that observed for this system. Zinc in $CaCl_2$ solution exhibits voltage overload for both anodic and cathodic processes at very low current densities, probably due to low solution conductivity.

b. Cadmium Electrode

(1) Dimethylformamide solution

The cyclic voltammogram for cadmium in $CaCl_2$ solution is shown in Figure 1 (CV-2963). The curve shows multiple anodic peaks and a single cathodic peak. The cathodic peak occurs 100 mv more positive than the first anodic peak. Similar results were obtained earlier in LiCl solution.

(2) Propylene carbonate solutions

Cadmium in LiCl + $LiClO_4$ solution shows only slight electrochemical activity, with no peak formation, similar to that observed earlier for zinc in this electrolyte.

The curve for cadmium in $LiClO_4 + AlCl_3$ solution is shown in Figure 2 (CV-3236). The curve shows a sharp anodic peak and two smaller cathodic peaks. Current densities are in the medium range. At faster scan rates only a single anodic and cathodic peak are observed. Further study would be required to interpret these results. The results in $CaCl_2$ solution are similar to those for the zinc electrode.

c. Molybdenum Electrode

(1) Dimethylformamide solution

Molybdenum is essentially inactive in $CaCl_2$ solution, as was observed earlier in LiCl solution.

(2) Propylene carbonate solutions

The CV curve for molybdenum in $LiClO_4 + AlCl_3$ solution shows a single broad anodic peak of medium high current density, and no cathodic activity. In $LiCl + LiClO_4$ solution, the curve for molybdenum shows low anodic activity and no cathodic activity. Molybdenum in $LiCl + AlCl_3$ solution results in voltage overload with high anodic and no cathodic current. In $MgCl_2$ and $CaCl_2$ solutions, anodic voltage overload results and no cathodic activity is indicated.

d. Indium Electrode

(1) Dimethylformamide solutions

The cyclic voltammogram for indium in $LiCl + AlCl_3$ solution is shown in Figure 3 (CV-3392). A complex anodic reaction is indicated by the multipeak positive current. Poor charge-discharge efficiency is predicted based on the low coulombic ratio (cathodic-to-anodic peak areas). Comparison of current peak height ratios at faster sweep rates indicates a soluble anodic product.

Anodic voltage overload results for indium in $CaCl_2$ solution.

(2) Propylene carbonate solutions

The cyclic voltammogram for indium in LiCl + $LiClO_4$ solution shows a low, broad anodic peak in the low current density range, and virtually no cathodic current.

Indium in $LiClO_4$ + $AlCl_3$ solution shows a sharp anodic peak in the medium high current density range, and broad multiple cathodic peaks. A similar curve for indium in LiCl + $AlCl_3$ solution is shown in Figure 4 (CV-3382).

The curve for indium in $MgCl_2$ solution is shown in Figure 5 (CV-2971) indicating a single anodic, and a double cathodic peak both in the high current density range. Indium in $CaCl_2$ solution shows voltage overload for both the anodic and cathodic sweeps.

e. Iron Electrode

(1) Dimethylformamide solution

Iron electrodes in $CaCl_2$ solution result in anodic voltage overload.

(2) Propylene carbonate solutions

Iron shows negligible activity in LiCl + $LiClO_4$ solution. In the case of $MgCl_2$ solution, iron shows a well formed anodic peak in the medium low range, followed by a lower broad peak. No cathodic reaction is evident, however. Very low anodic and cathodic activity occurs for iron in $CaCl_2$ solution, and no peaks are observed.

Iron electrodes in LiCl + $AlCl_3$ solution exhibit complex anodic peaks in the medium high current density range, with low cathodic activity. Similar complex anodic peaks occur for iron in $LiClO_4$ + $AlCl_3$ solution. Cathodic activity is indicated at the extreme negative end of the cathodic scan resulting in more than 1 volt peak-to-peak separation.

f. Vanadium Electrode

(1) Dimethylformamide solutions

Vanadium electrodes indicate very high anodic activity in LiCl solution causing anodic current overload of the instrumentation. The solution turns a dark red color indicating anodic dissolution of the electrode. Cathodic current is nil. Vanadium in $CaCl_2$ solution results in anodic voltage overload. A red discoloration of the solution was noted, as well as the formation of a black reaction product on the working electrode. Anodic voltage overload results for vanadium in $LiClO_4$ and $LiCl + AlCl_3$ solutions. Again, cathodic current is negligible. The sweep curve for vanadium in $Mg(ClO_4)_2$ solution shows a sharp, very high current density anodic peak and virtually no cathodic activity. This is shown in Figure 6 (CV-3444).

(2) Propylene carbonate solutions

No electrochemical activity is observed for vanadium in $LiCl + LiClO_4$ solution. The curve for vanadium in $LiClO_4$ solution shows a single sharp anodic high current density peak and only low cathodic activity. Vanadium in $LiClO_4 + AlCl_3$ solution shows a single, sharp anodic peak in the high current density range and relatively no cathodic activity. In $LiCl + AlCl_3$ solution, vanadium electrodes exhibit anodic voltage overload due to high current. Red discoloration of the solution, with negligible cathodic reaction, indicates excessive anodic dissolution. Vanadium in $CaCl_2$ solution shows very low anodic and no cathodic activity.

g. Chromium Electrode

(1) Dimethylformamide solutions

The curve for chromium in $Mg(ClO_4)_2$ solution is shown in Figure 7 (CV-3449). A single anodic peak of high current density with virtually no reduction current is evident. Chromium electrodes in $LiClO_4$, LiCl, and $LiCl + AlCl_3$ solutions result in anodic voltage overload with no cathodic activity.

(2) Propylene carbonate solutions

Chromium in LiCl + $AlCl_3$ solution show multipeak anodic activity in the medium high range and low cathodic activity. Low anodic and very low cathodic activity is indicated in $LiClO_4$ solution.

h. Manganese Electrode

(1) Dimethylformamide solutions

Manganese electrodes in chloride and perchlorate solutions show a large voltage spread between anodic and cathodic peaks indicating high activation polarization. In the case of LiCl + $AlCl_3$ solution, the curves show a broad, high anodic peak, with low cathodic activity at the negative extreme of the voltage range. Very low anodic and cathodic activity at the scan limits is observed also for $Mg(ClO_4)_2$. Curves for $LiClO_4$ solution show a single, very high anodic peak at the positive extreme, but no cathodic activity within the total scan. The curve for manganese in LiCl solution shows a single, anodic peak and multiple broad cathodic peaks. Peak current densities fall in the low range, and peak-to-peak voltage separation is greater than 0.5 v. The curve is shown in Figure 8 (CV-3315).

(2) Propylene carbonate solutions

Manganese in LiCl + $AlCl_3$ solution shows a medium low, current density anodic peak and no cathodic activity. Low anodic currents and no cathodic activity is indicated in $LiClO_4$ solution.

2. Systems Involving Fluoride Electrolytes

a. Zinc Electrode

(1) Dimethylformamide solutions

Zinc electrodes in PF_5 solution give voltage overload caused by a combination of very high anodic current and low solution conductivity. Cathodic voltage overload is obtained in $Mg(PF_6)_2$ solution. The cyclic voltammogram for zinc in $Ca(PF_6)_2$ solution shows a single broad, high current density anodic peak. The reduction reaction is initiated at the same potential as the oxidation reaction, forming a well-defined cathodic peak. 200 mv negative to this peak, however, erratic peak behavior is obtained, which may be related to the observed continuous dislodging of reaction product from the electrode.

The curve for zinc in $LiBF_4$ solution is shown in Figure 9 (CV-3272). A secondary oxidation process is indicated. The cathodic peak occurring 0.4 v cathodic to the major anodic peak appears clean, although, a second cathodic reaction is indicated at the extreme end of the negative range. Peak current densities fall in the medium high range. Measurements in BF_3, $Mg(BF_4)_2$, and $Ca(BF_4)_2$ solutions result in anodic and cathodic voltage overload with very high cathodic current densities.

(2) Propylene carbonate solutions

Zinc in PF_5 solution shows a broad, low current density cathodic peak, and a medium low anodic with no tendency towards peaking. The curve for zinc in $Mg(PF_6)_2$ solution is shown in Figure 10 (CV-3134). The single anodic and cathodic peaks fall in the medium high current density range, and are seen to be broad and highly polarized as evidenced by a peak-to-peak separation greater than 1 volt.

Zinc electrodes in $LiBF_4$ solution show a sharp anodic peak followed by very erratic non-reproducible cathodic activity. The erratic behavior may be due to sudden changes, such as cracking of the electrode surface layer, exposing

new electroactive surface. A black reaction product forms on the working electrode. Peak current densities are in the medium low range.

Zinc in $Ca(BF_4)_2$ solution shows broad, single anodic and cathodic peaks separated by 0.8 v. Peak current densities are in the high and medium high range respectively. In $Ca(PF_6)_2$ solution, the curve shows a medium low anodic and a medium high cathodic peak. Small random oscillations are exhibited, possibly caused by erratic surface changes. Voltage overload occurs in $Mg(BF_4)_2$ solutions as a result of very high current densities.

b. Cadmium Electrode

(1) Dimethylformamide solutions

The cyclic voltammogram for cadmium in PF_5 solution shows a broad, poorly defined irreproducible anodic peak of very high current density, and a medium low current density cathodic peak. Anodic-to-cathodic peak voltage separation is greater than 1 volt. Voltage overload results in $Mg(PF_6)_2$ and $Ca(PF_6)_2$ solutions, as a result of a combination of very high anodic and cathodic activity and low solution conductivity.

Measurements on cadmium in $LiBF_4$ solutions caused instrumental oscillation and voltage overload near the extremes of the voltage range. These oscillations are no doubt set off by sudden changes in electrode geometry, in combination with high current densities, resulting in impedance mismatch and affecting the response of the potentiostat. A cyclic voltammogram was recorded for this system by setting voltage limits at only ±0.3 v relative to the o.c.v. The curve is a good example of a high current density reversible system, and is shown in Figure 11 (CV-3273). Cadmium in BF_3, $Mg(BF_4)_2$, and $Ca(BF_4)_2$ solutions result in voltage overload for both anodic and cathodic sweeps.

(2) Propylene carbonate solutions

Cadmium electrodes in PF_5 solution yield results similar to those observed for zinc in this electrolyte. A medium high cathodic peak is obtained, with

no tendency for anodic peak formation. The curve is shown in Figure 12 (CV-3006). Cadmium in $Mg(PF_6)_2$ solution results in voltage overload.

Voltage overload resulted for cadmium in $Ca(PF_6)_2$, $Mg(BF_4)_2$ and $Ca(BF_4)_2$ solutions. In $Mg(BF_4)_2$ solution, overload results for both anodic and cathodic sweeps. In $Ca(PF_6)_2$ and $Ca(BF_4)_2$ solutions the overload condition is encountered only on the anodic sweep.

Cadmium in $LiBF_4$ solution exhibits voltage overload caused by system oscillations similar to that described above for the Cd/DMF-$LiBF_4$ system. Very high anodic and cathodic currents were recorded. Additional measurements are warranted for this system.

c. Molybdenum Electrode

(1) Dimethylformamide solutions

Curves for molybdenum electrodes in PF_5 solution show two very low but distinct anodic peaks, and no cathodic activity. In $LiPF_6$ solution, two anodic peaks are again formed, but closer together than in PF_5 solution. Low cathodic activity is indicated in $LiPF_6$ solution, with two peaks again evident. Charge-to-discharge voltage separation is excessively large however. Voltage overload occurs in both $Mg(PF_6)_2$ and $Ca(PF_6)_2$ solutions.

The results for molybdenum electrodes in $LiBF_4$ solution indicate anodic activity in the medium high current density range, but no cathodic activity. Voltage overload results in BF_3, $Mg(BF_4)_2$ and $Ca(BF_4)_2$ solutions with high currents on the anodic sweep, but with no current on the cathodic sweep.

(2) Propylene carbonate solutions

Molybdenum shows no activity in PF_5 solution, within the normal scanning range (+1.0 to -1.0v), but in the range 0 to +2.0 v, anodic voltage overload occurs. A medium high anodic peak is obtained in $LiPF_6$ solution, and the cathodic peak is of low current density and separated by more than 1.0 v

from the anodic reaction. Anodic voltage overload results for molybdenum in $Mg(PF_6)_2$ solution. Molybdenum in $LiBF_4$ solution shows results similar to those observed in dimethylformamide solution. Medium high anodic current is obtained with no tendency towards peak formation. A low cathodic current occurs at -1.0 v. Similar results with lower current densities are observed for molybdenum in $Ca(BF_4)_2$, but with lower current densities.

Voltage overload caused by very high anodic currents results for molybdenum in $Mg(BF_4)_2$ and $Ca(PF_6)_2$ solutions. The cathodic current for both of these systems is nil.

d. Indium Electrode

(1) Dimethylformamide solutions

The cyclic voltammogram for indium in PF_5 solution shows a high anodic current with no tendency for peak formation. No reduction reaction is evident. The solution becomes dark brown during cycling. Indium in $LiPF_6$ solution shows very high anodic activity as indicated in Figure 13 (CV-3036). The cathodic current is in the very low range, and is limited by the anodic dissolution of the indium working electrode as evidenced by darkening of the solution and plating out of a metal (presumably indium) on the counterelectrode. Sweep rate behavior also indicates a soluble cathode. Voltage overload results in $Mg(PF_6)_2$ and $Ca(PF_6)_2$ solutions, again due to very high anodic activity and low solution conductance.

The curve for indium in $LiBF_4$ solution shows very high anodic and medium low cathodic activity. As seen in Figure 14 (CV-3282) the anodic peak area is much larger than the cathodic peak area (by roughly a factor of a hundred) indicating poor charge-discharge efficiency. Voltage overload results for both anodic and cathodic sweeps due to very high currents and low conductivity in BF_3, $Mg(BF_4)_2$, and $Ca(BF_4)_2$ solutions.

(2) Propylene carbonate solutions

The electrochemical behavior of indium electrodes in PF_5 solution is similar to that observed for PF_5 in dimethylformamide. Indium in $LiPF_6$ solution shows high anodic and medium high cathodic activity, accompanied by excessive dissolution of the cathodic material. Metal deposition, presumably indium, is observed on the counterelectrode. Anodic voltage overload results for indium electrodes in $Mg(PF_6)_2$ solution.

The cyclic voltammogram for indium in $LiBF_4$ solution is shown in Figure 15 (CV-3179). The electrode characteristics indicated in this curve are an improvement over that in Figure 14 (CV-3282) for dimethylformamide solution. Still, the large peak-to-peak voltage separation (0.9v), and low cathodic-to-anodic coulombic ratio, are not favorable from the standpoint of secondary battery operation.

Indium in $Ca(PF_6)_2$, $Ca(BF_4)_2$ and $Mg(BF_4)_2$ all results in voltage overload caused by very high anodic and cathodic currents and low solution conductivity.

e. Iron Electrode

(1) Dimethylformamide solutions

Iron in PF_5 solution causes voltage overload as a result of high anodic activity and low solution conductance. High anodic and cathodic activity occurs in $LiPF_6$, $Mg(PF_6)_2$ and $Ca(PF_6)_2$ solutions. The broad multiple peaks and large voltage separation between anodic and cathodic reactions in all three systems make them unsatisfactory for secondary battery application.

Iron electrodes in $LiBF_4$ solution show a sharp anodic peak of medium high current density and very low cathodic activity. In $Mg(BF_4)_2$ and $Ca(BF_4)_2$ solutions, iron electrodes show sharp anodic peaks of very high current density and low cathodic activity. Voltage separation is greater than 1 volt. The cyclic voltammogram for iron in $Mg(BF_4)_2$ solution is shown in Figure 16

(CV-3328). Voltage overload results in BF_3 solution on the anodic sweep, with high anodic and cathodic currents.

(2) Propylene carbonate solutions

The cyclic voltammogram for iron in PF_5 solution indicates low anodic and cathodic activity with no peak formation. The curve for iron in $LiPF_6$ solution is shown in Figure 17 (CV-3061) and is the best of the iron systems examined to date. Peak currents are in the medium low range, peak-to-peak separation is 0.5 v, and the charge-discharge efficiency is 86%. Iron in $Mg(PF_6)_2$ solution shows broad, low anodic peak and very low cathodic activity with no peak formation.

The cyclic voltammogram for iron in $LiBF_4$ solutions is shown in Figure 18 (CV-3189). The curve shows single anodic and cathodic peaks of medium low current densities, and 1.4 v peak-to-peak separation. The large voltage separation indicates high activation polarization. Similar results are obtained for iron in $Mg(BF_4)_2$, $Ca(BF_4)_2$ and $Ca(PF_6)_2$ solutions.

f. Vanadium Electrode

(1) Dimethylformamide solutions

Vanadium in PF_5 solution results in voltage overload. Sharp anodic peaks in the medium low current density range, with repeat peaks at the same potential on the reverse sweep, occur in $LiPF_6$, $Mg(PF_6)_2$, and $Ca(PF_6)_2$ solutions. In each case, a low cathodic peak is observed, separated by greater than 1 volt from the anodic peak. The curve for $LiPF_6$ is shown in Figure 19 (CV-3046). The results for vanadium in KPF_6 solution are similar except that no cathodic activity or repeat peaks are observed.

The voltammograms for vanadium electrodes in $LiBF_4$, $Mg(BF_4)_2$, $Ca(BF_4)_2$, and in BF_3 solutions show low to very low anodic and cathodic activity. In

general, results for vanadium, in fluoride electrolyte, show anodic activity decreasing after the first cycle. Continued cycling yields reproducibility only at low or very low current density levels.

(2) Propylene carbonate solutions

Vanadium after a few cycles exhibits very low electrochemical activity in PF_5, $LiPF_6$, KPF_6, or $Mg(PF_6)_2$ and $Ca(PF_6)_2$ solutions of propylene carbonate.

In the case of $LiBF_4$, $Mg(BF_4)_2$, and $Ca(BF_4)_2$ solutions, vanadium exhibits low or very low anodic and cathodic activity following the first few cycles. A typical curve obtained after several cycles is shown in Figure 20 (CV-3171).

g. Chromium Electrode

(1) Dimethylformamide solutions

The curve for chromium in $LiPF_6$ solution shows a single sharp anodic peak of medium low current density range, and no cathodic peak. Cathodic activity of less than 2 ma/cm^2 is indicated at the extreme negative voltage range. Similar results are obtained for KPF_6 solutions. Chromium electrodes in $LiBF_4$ and in BF_3 solutions result in anodic voltage overload accompanied by high currents. Cathodic currents are negligible in both cases.

(2) Propylene carbonate solutions

The curve for chromium in KPF_6 solution shows low anodic and very low cathodic activity with no current peaks. Similar results occur in $Ca(PF_6)_2$ solution. Chromium electrodes in PF_5 and $Ca(BF_4)_2$ solutions result in voltage overload with high anodic currents. No reduction reaction is evidenced.

h. Managese Electrode

(1) Dimethylformamide solutions

The curve for manganese in $LiPF_6$ solution shows single anodic and cathodic peaks of high current density. High activation polarization is indicated by

0.9 v peak-to-peak voltage separation as seen in Figure 21 (CV-3303). Plating of a metal on the counterelectrode indicates that some anodic dissolution is occurring. The curve obtained in KPF_6 solution is shown in Figure 22 (CV-3439).

Manganese in $LiBF_4$ solution shows single anodic and cathodic peaks. The sweep rate dependence of the anodic and cathodic peaks indicates a soluble anodic product. Peak-to-peak voltage separation is 0.7 v. Voltage overload results on both anodic and cathodic sweeps for manganese in BF_3, $Mg(BF_4)_2$, $Ca(BF_4)_2$, and PF_5 solutions.

(2) Propylene carbonate solutions

Manganese in KPF_6 and $Ca(PF_6)_2$ solutions shows low cathodic activity. The anodic current in the case of KPF_6 is in the medium low range, although no peak results. In $Ca(PF_6)_2$ solution a broad anodic peak in the low current density range is observed.

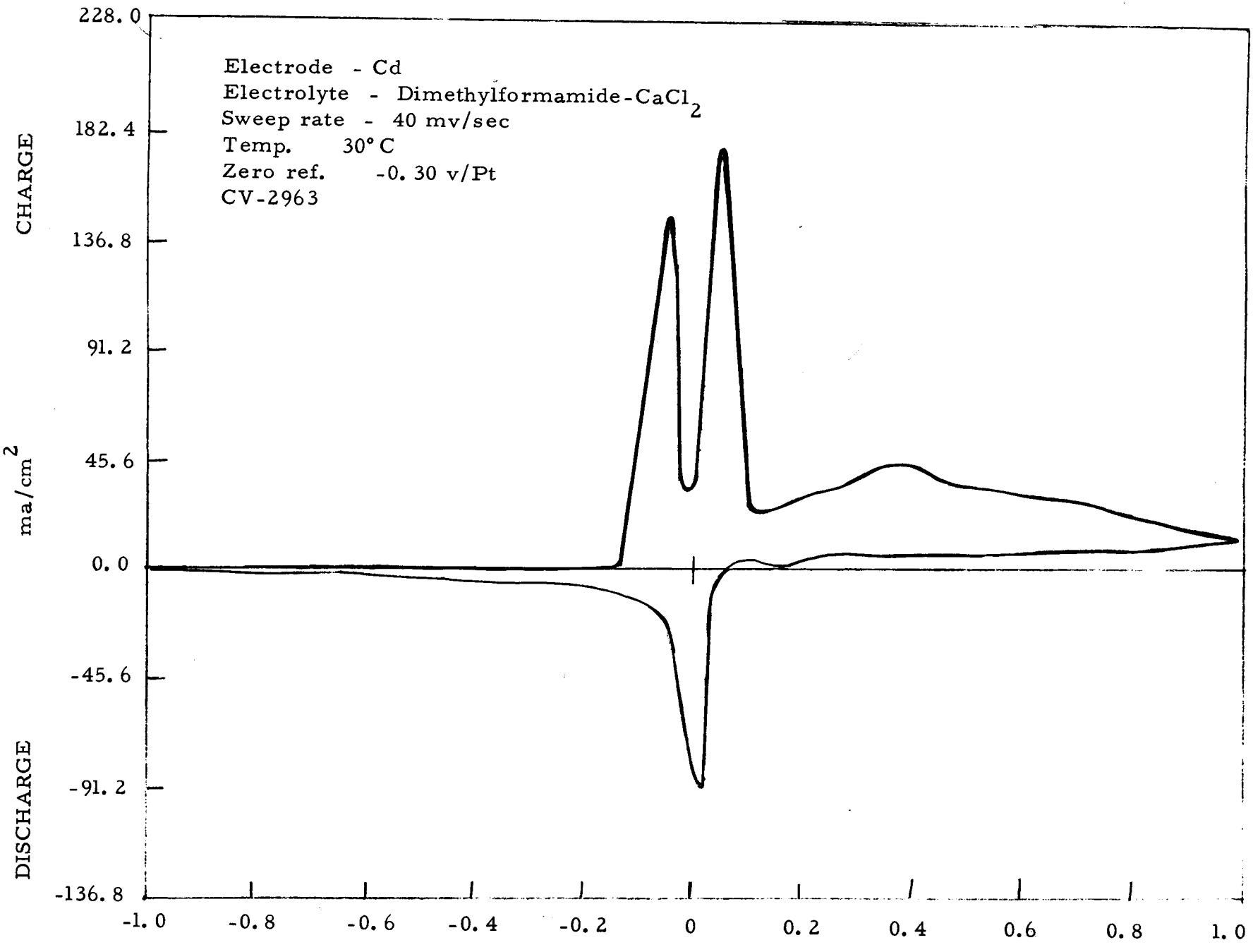
Electrode - Cd
Electrolyte - Dimethylformamide-$CaCl_2$
Sweep rate - 40 mv/sec
Temp. 30° C
Zero ref. -0.30 v/Pt
CV-2963
228.0
182.4
136.8
91.2
45.6
0.0
-45.6
-91.2
-136.8
CHARGE
DISCHARGE
ma/cm^2
-1.0
-0.8
-0.6
-0.4
-0.2
0
0.2
0.4
0.6
0.8
1.0
VOLTS POLARIZATION

Figure 1

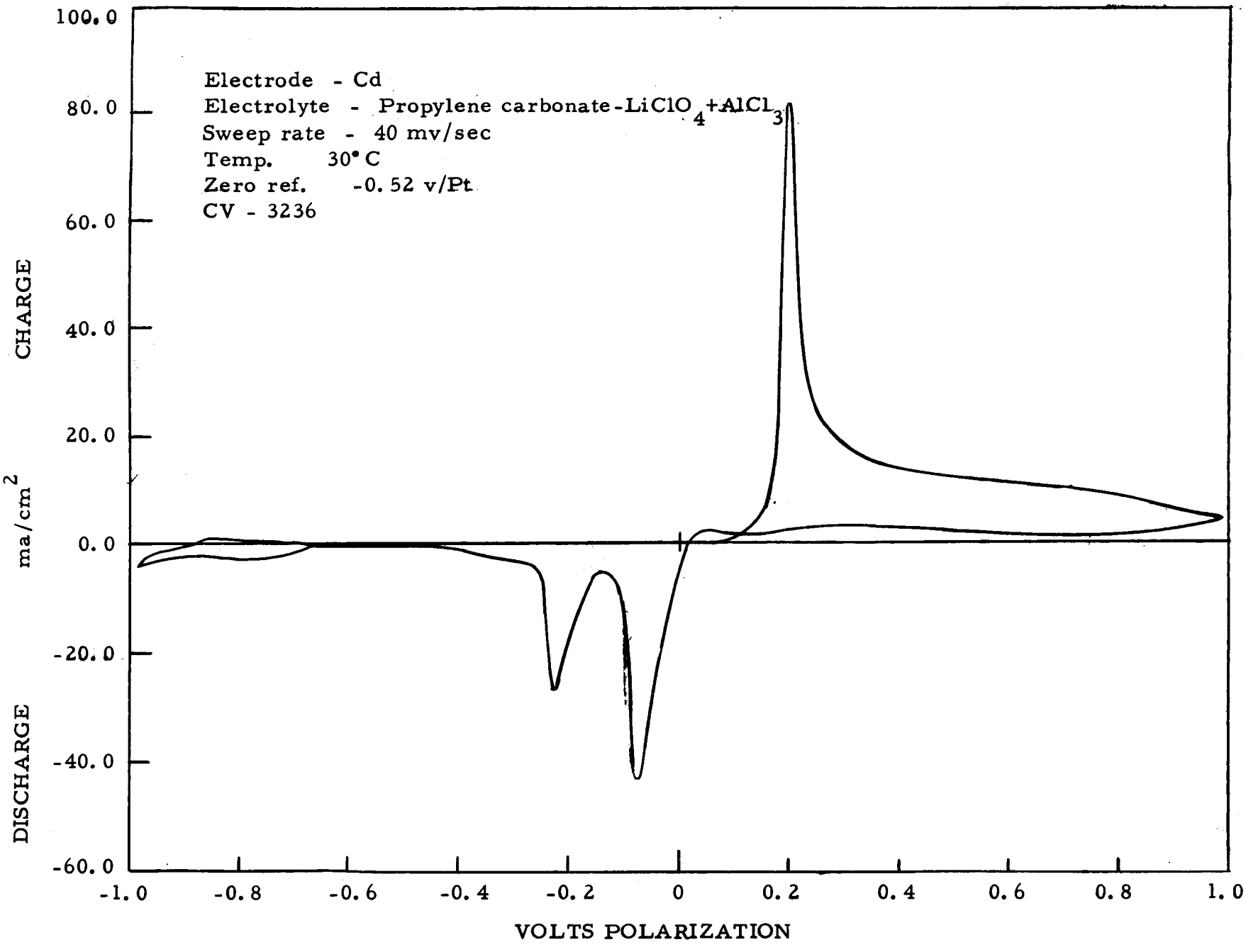
Electrode - Cd
Electrolyte - Propylene carbonate-$LiClO_4$+$AlCl_3$
Sweep rate - 40 mv/sec
Temp. 30° C
Zero ref. -0.52 v/Pt
CV - 3236
100.0
80.0
60.0
40.0
20.0
0.0
-20.0
-40.0
-60.0
CHARGE
DISCHARGE
ma/cm^2
-1.0
-0.8
-0.6
-0.4
-0.2
0
0.2
0.4
0.6
0.8
1.0
VOLTS POLARIZATION

Figure 2

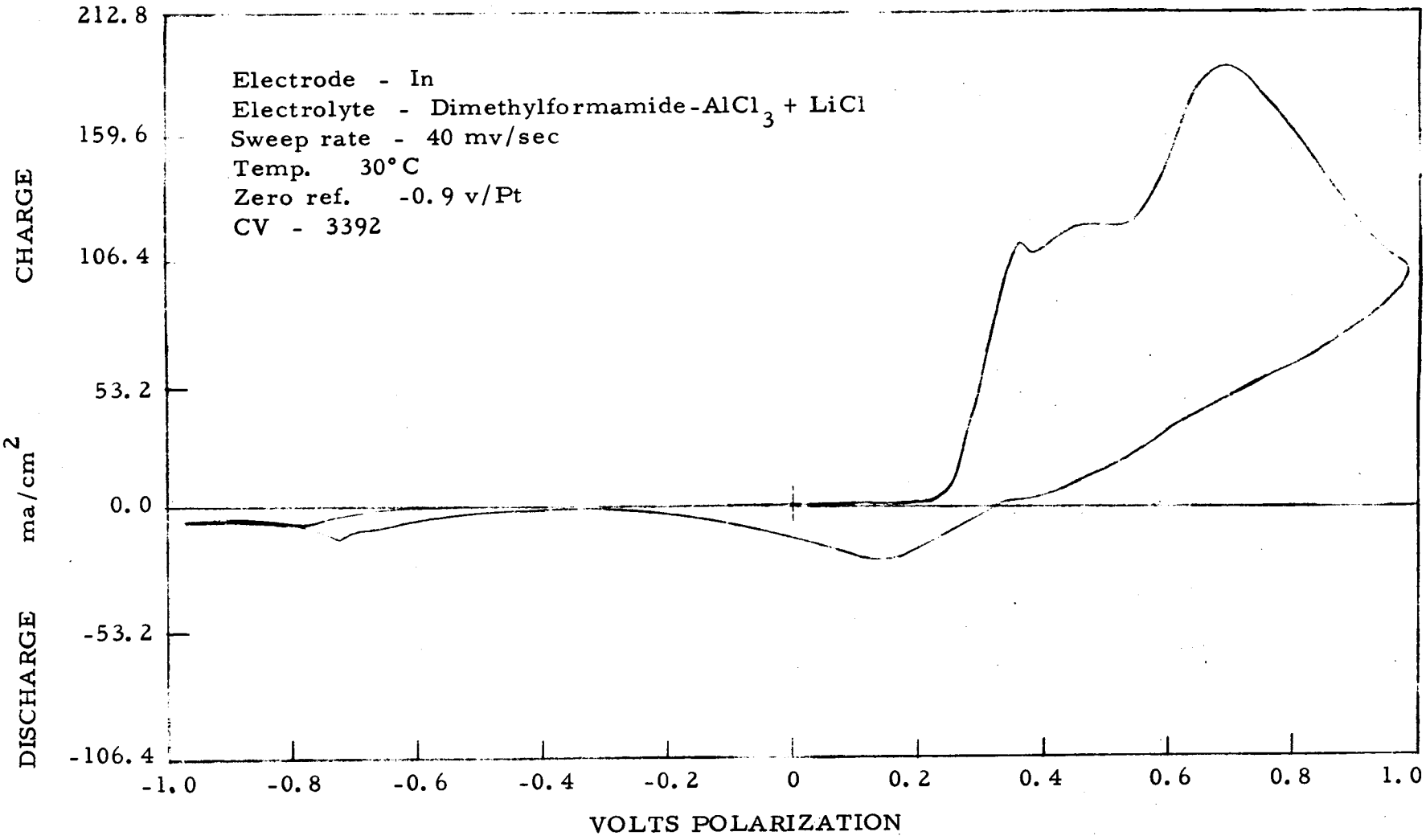
Electrode - In
Electrolyte - Dimethylformamide-AlCl3 + LiCl
Sweep rate - 40 mv/sec
Temp. 30° C
Zero ref. -0.9 v/Pt
CV - 3392
212.8
159.6
106.4
53.2
0.0
-53.2
-106.4
CHARGE
DISCHARGE
ma/cm2
-1.0
-0.8
-0.6
-0.4
-0.2
0
0.2
0.4
0.6
0.8
1.0
VOLTS POLARIZATION

Figure 3

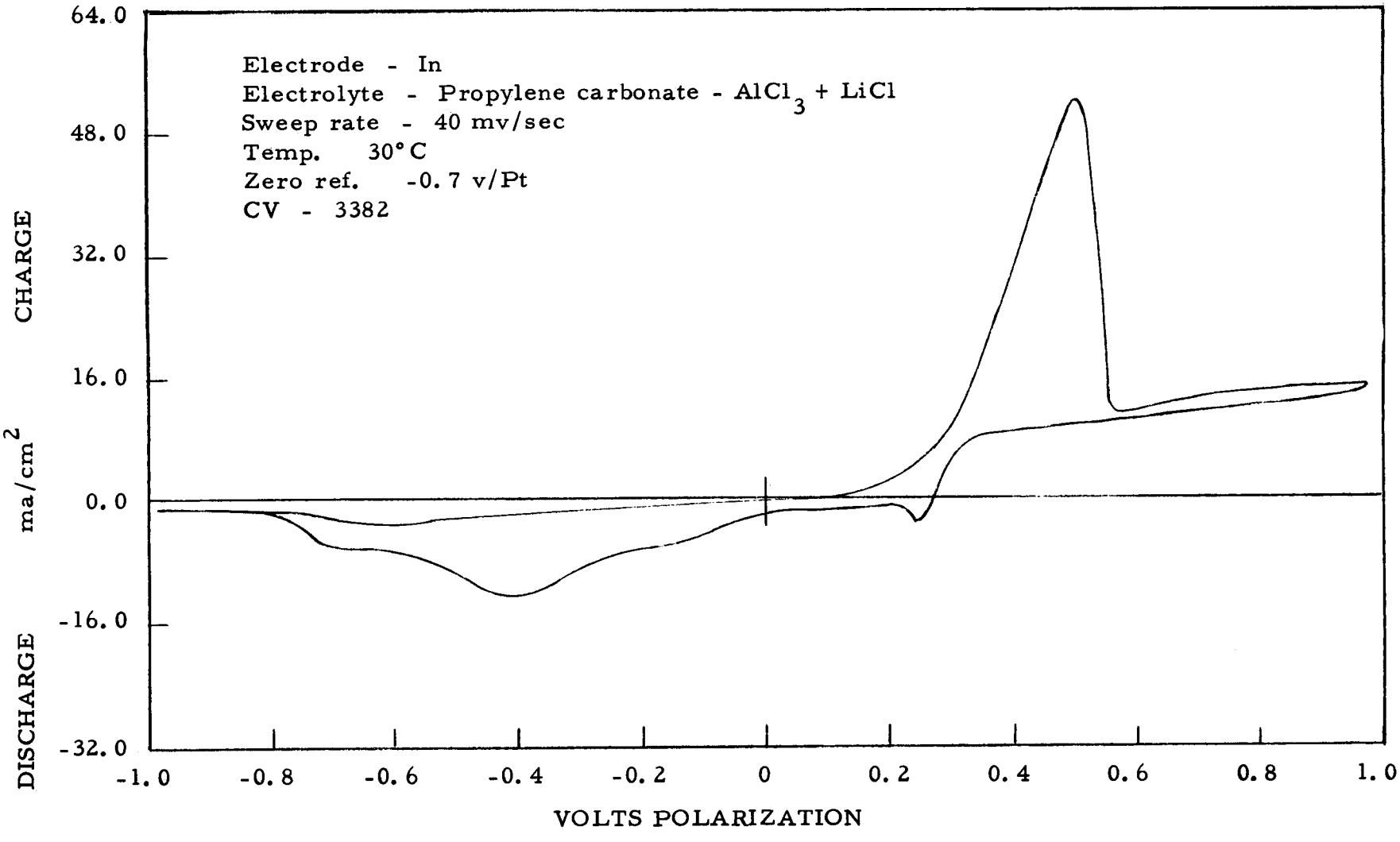
Electrode - In
Electrolyte - Propylene carbonate - $AlCl_3$ + LiCl
Sweep rate - 40 mv/sec
Temp. 30° C
Zero ref. -0.7 v/Pt
CV - 3382
64.0
48.0
32.0
16.0
0.0
-16.0
-32.0
CHARGE
DISCHARGE
ma/cm^2
-1.0
-0.8
-0.6
-0.4
-0.2
0
0.2
0.4
0.6
0.8
1.0
VOLTS POLARIZATION

Figure 4

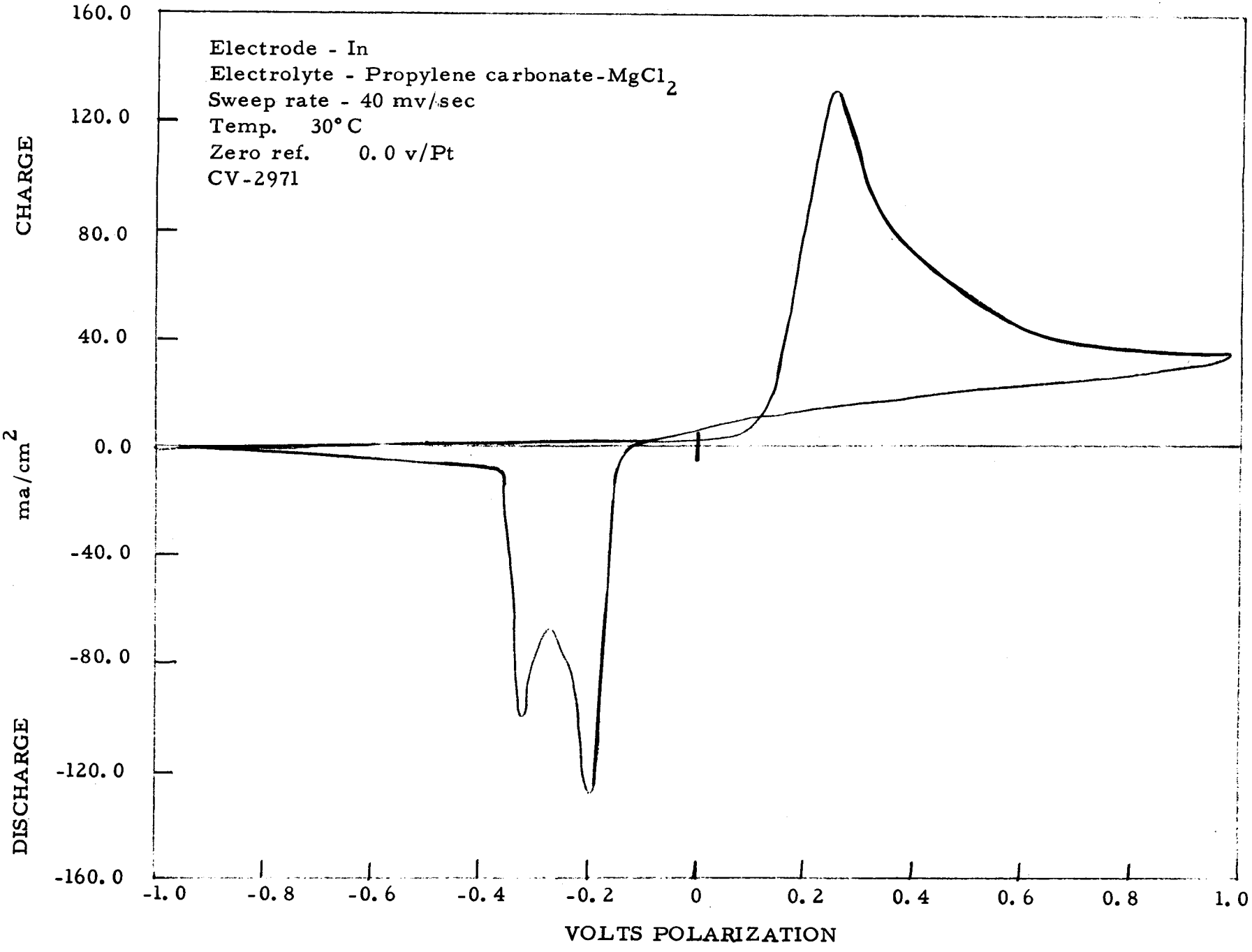
Electrode - In
Electrolyte - Propylene carbonate-$MgCl_2$
Sweep rate - 40 mv/sec
Temp. 30° C
Zero ref. 0.0 v/Pt
CV-2971
160.0
120.0
80.0
40.0
0.0
-40.0
-80.0
-120.0
-160.0
CHARGE
DISCHARGE
ma/cm^2
-1.0
-0.8
-0.6
-0.4
-0.2
0
0.2
0.4
0.6
0.8
1.0
VOLTS POLARIZATION

Figure 5

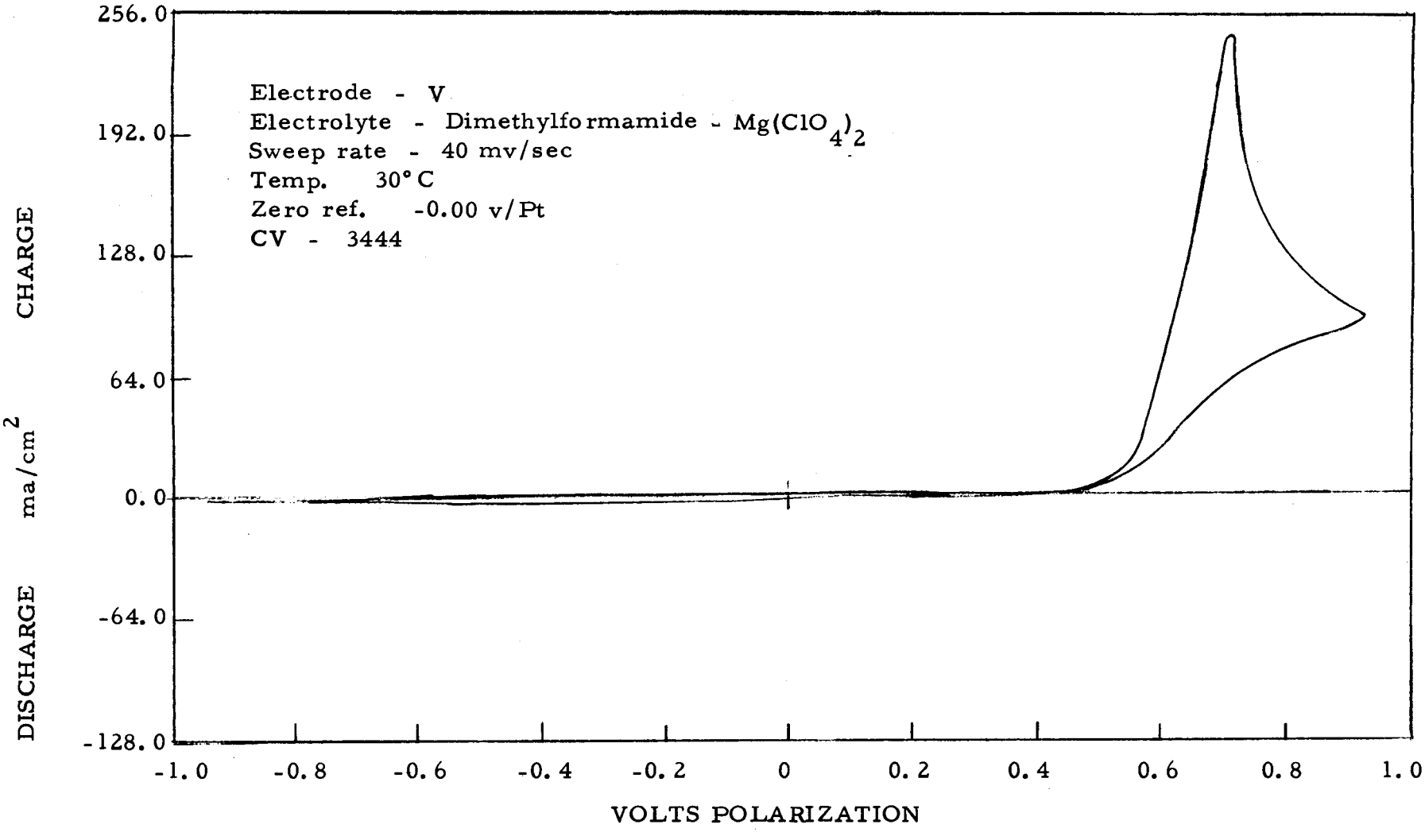
Electrode - V
Electrolyte - Dimethylformamide - $Mg(ClO_4)_2$
Sweep rate - 40 mv/sec
Temp. 30° C
Zero ref. -0.00 v/Pt
CV - 3444
256.0
192.0
128.0
64.0
0.0
-64.0
-128.0
CHARGE
DISCHARGE
ma/cm^2
-1.0
-0.8
-0.6
-0.4
-0.2
0
0.2
0.4
0.6
0.8
1.0
VOLTS POLARIZATION

Figure 6

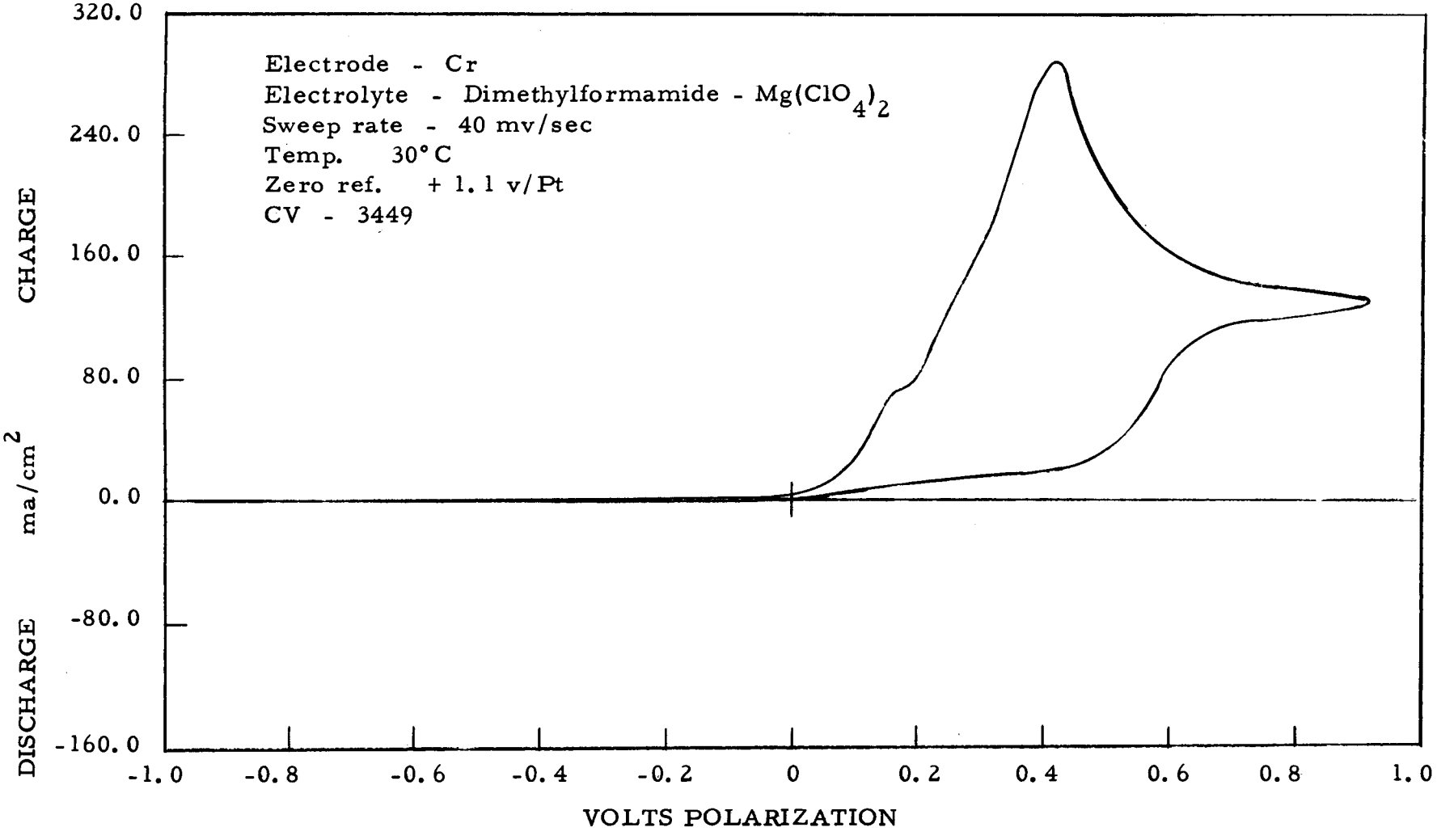
Electrode - Cr
Electrolyte - Dimethylformamide - $Mg(ClO_4)_2$
Sweep rate - 40 mv/sec
Temp. 30°C
Zero ref. + 1.1 v/Pt
CV - 3449
320.0
240.0
160.0
80.0
0.0
-80.0
-160.0
CHARGE
DISCHARGE
ma/cm^2
-1.0
-0.8
-0.6
-0.4
-0.2
0
0.2
0.4
0.6
0.8
1.0
VOLTS POLARIZATION

Figure 7

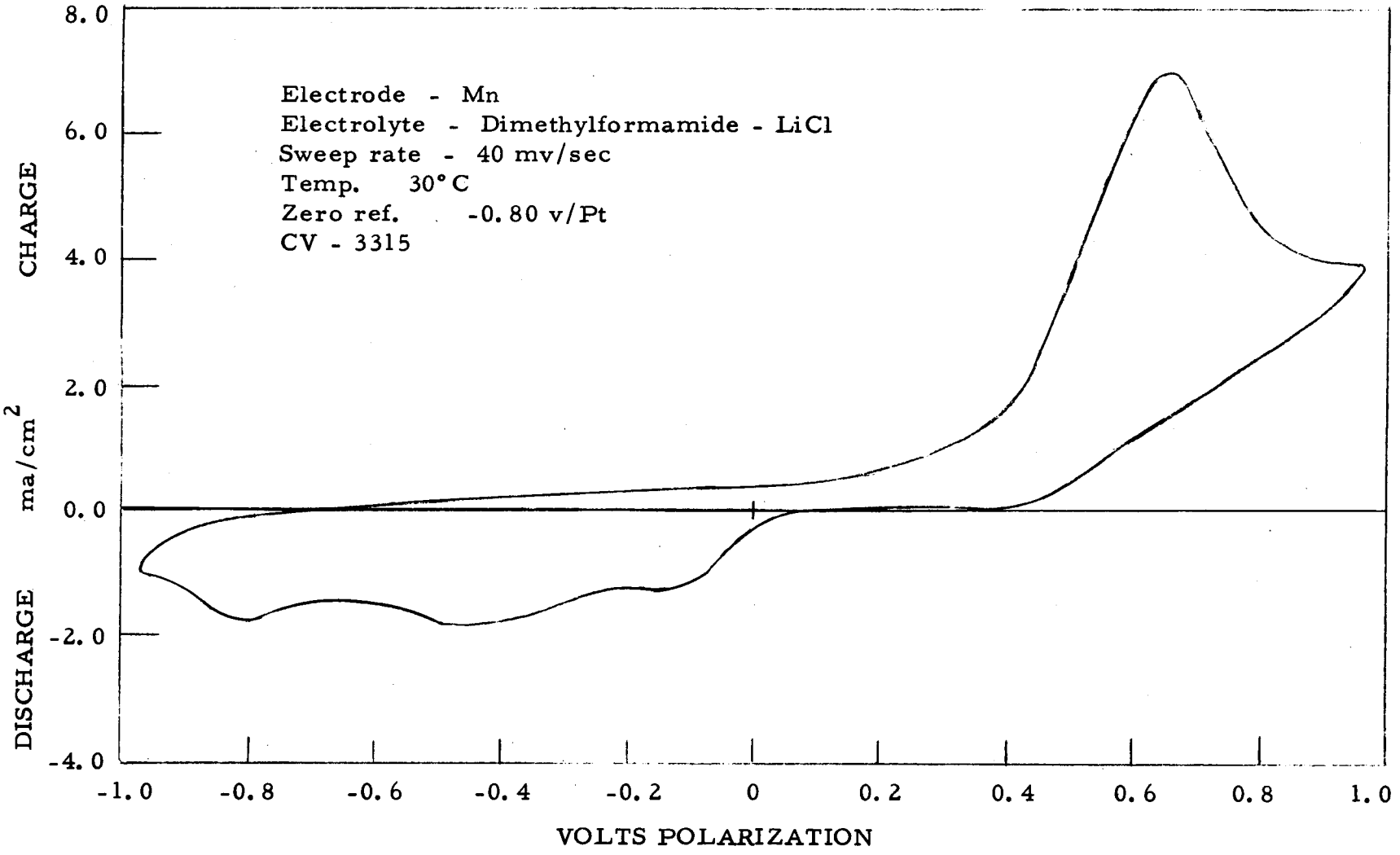
Electrode - Mn
Electrolyte - Dimethylformamide - LiCl
Sweep rate - 40 mv/sec
Temp. 30° C
Zero ref. -0.80 v/Pt
CV - 3315
CHARGE
DISCHARGE
ma/cm 2
8.0
6.0
4.0
2.0
0.0
-2.0
-4.0
-1.0
-0.8
-0.6
-0.4
-0.2
0
0.2
0.4
0.6
0.8
1.0
VOLTS POLARIZATION

Figure 8

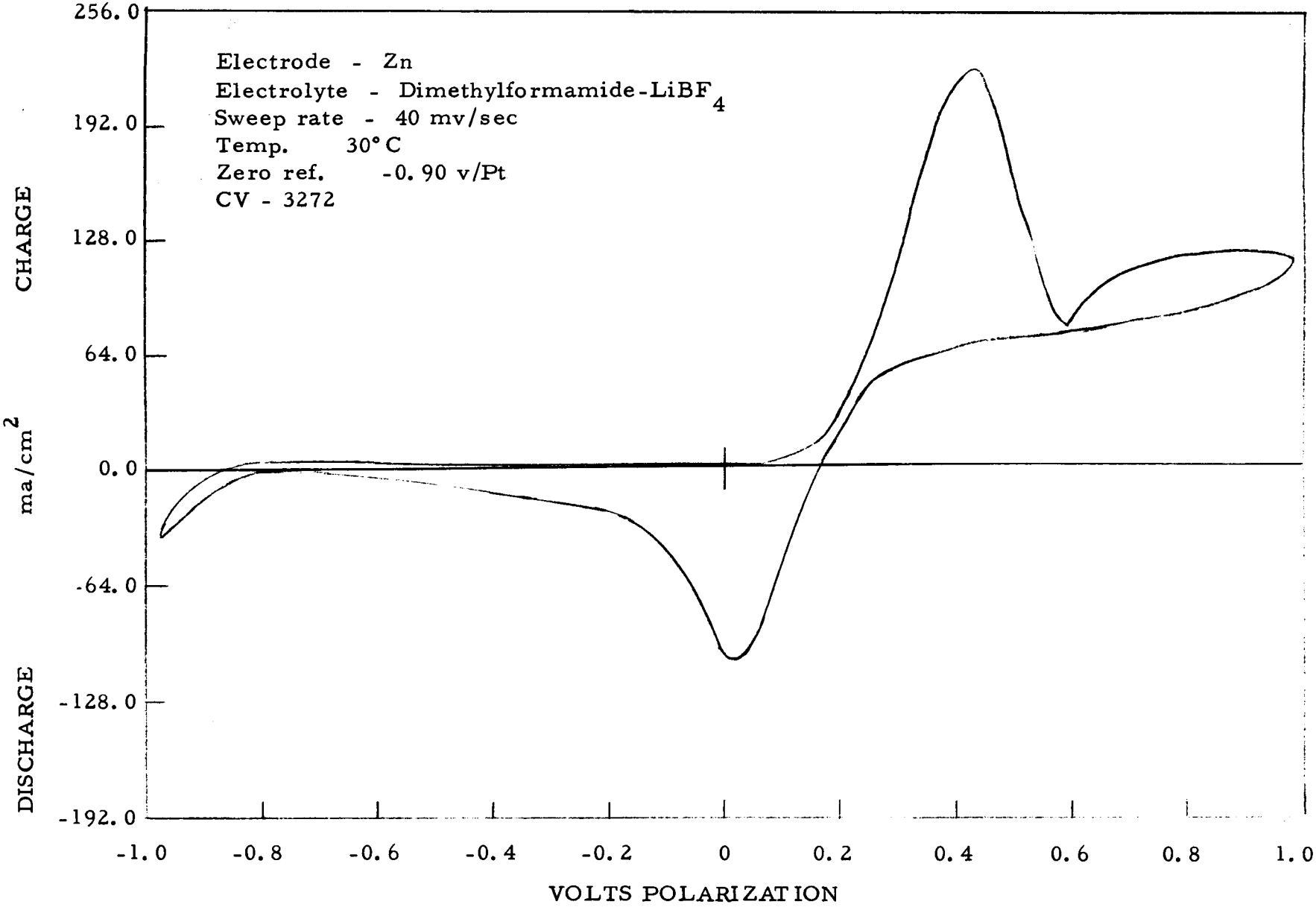
Electrode - Zn
Electrolyte - Dimethylformamide-LiBF4
Sweep rate - 40 mv/sec
Temp. 30° C
Zero ref. -0.90 v/Pt
CV - 3272
256.0
192.0
128.0
64.0
0.0
-64.0
-128.0
-192.0
CHARGE
DISCHARGE
ma/cm2
-1.0
-0.8
-0.6
-0.4
-0.2
0
0.2
0.4
0.6
0.8
1.0
VOLTS POLARIZATION

Figure 9

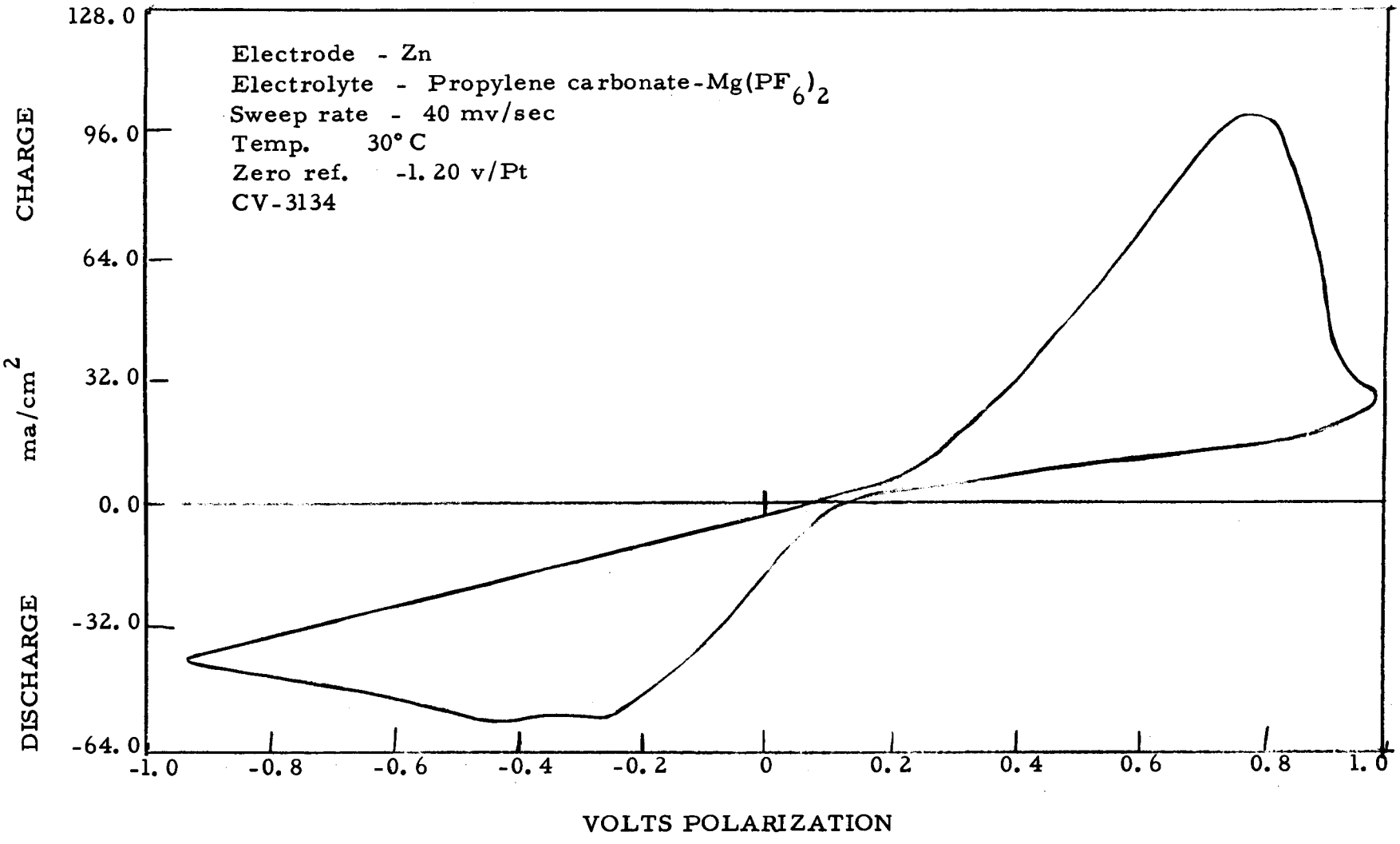
Electrode - Zn
Electrolyte - Propylene carbonate-Mg(PF6)2
Sweep rate - 40 mv/sec
Temp. 30° C
Zero ref. -1.20 v/Pt
CV-3134
CHARGE
DISCHARGE
ma/cm2
128.0
96.0
64.0
32.0
0.0
-32.0
-64.0
-1.0
-0.8
-0.6
-0.4
-0.2
0
0.2
0.4
0.6
0.8
1.0
VOLTS POLARIZATION

Figure 10

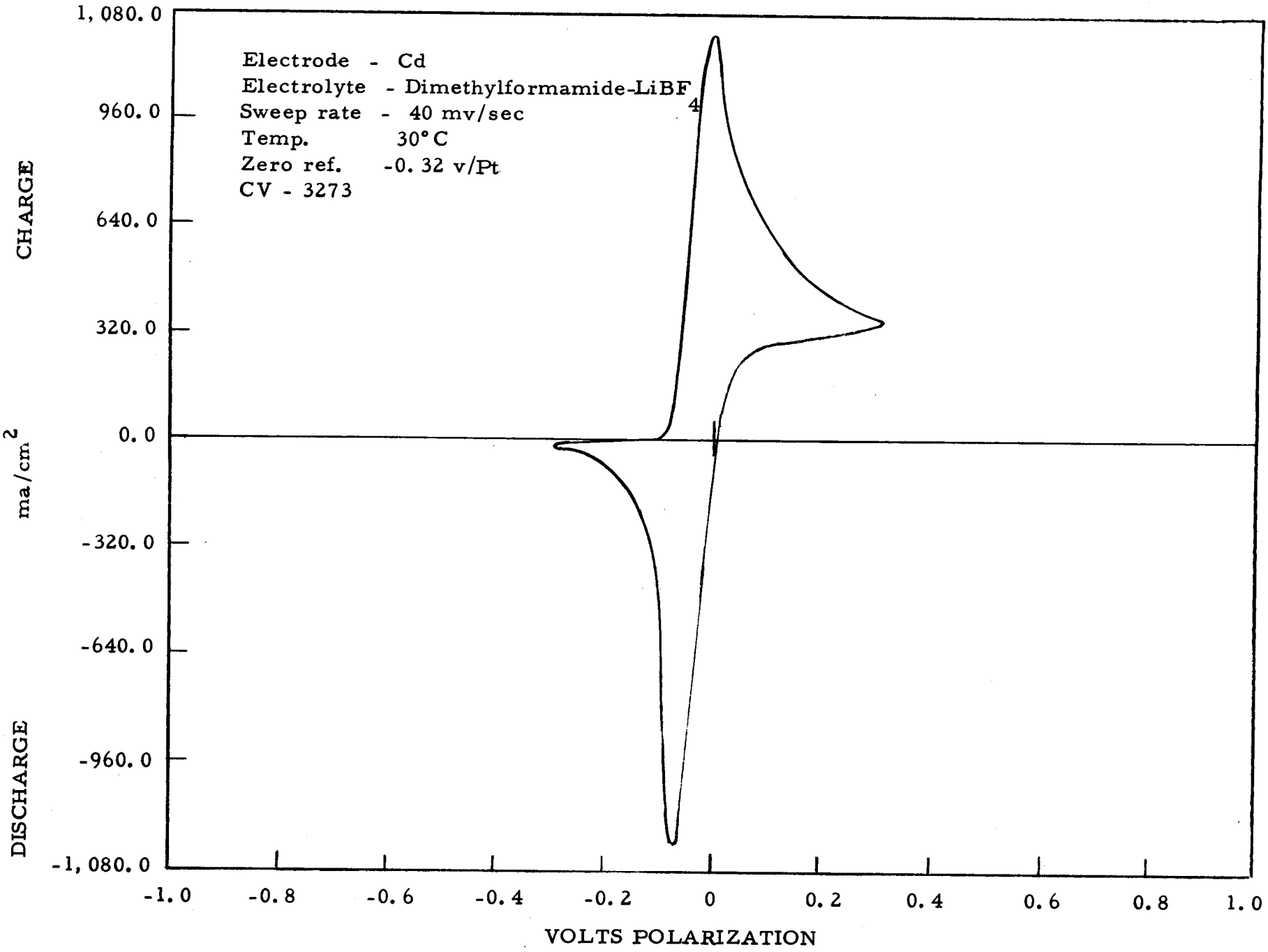
Electrode - Cd
Electrolyte - Dimethylformamide-LiBF4
Sweep rate - 40 mv/sec
Temp. 30° C
Zero ref. -0.32 v/Pt
CV - 3273
1,080.0
960.0
640.0
320.0
0.0
-320.0
-640.0
-960.0
-1,080.0
CHARGE
DISCHARGE
ma/cm2
-1.0
-0.8
-0.6
-0.4
-0.2
0
0.2
0.4
0.6
0.8
1.0
VOLTS POLARIZATION

Figure 11

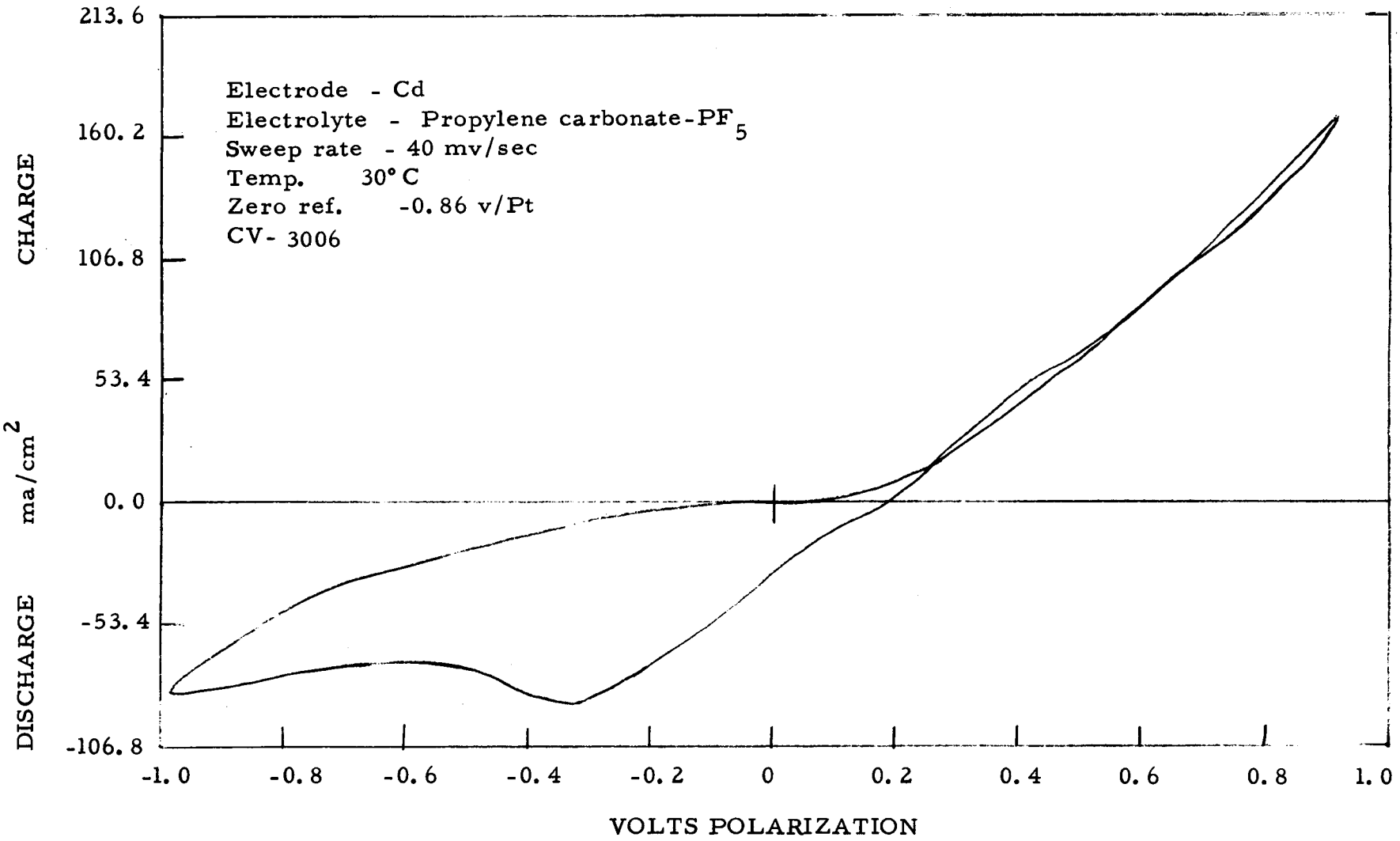
213.6
160.2
106.8
53.4
0.0
-53.4
-106.8
CHARGE
DISCHARGE
ma/cm 2
Electrode - Cd
Electrolyte - Propylene carbonate-PF5
Sweep rate - 40 mv/sec
Temp. 30° C
Zero ref. -0.86 v/Pt
CV- 3006
-1.0
-0.8
-0.6
-0.4
-0.2
0
0.2
0.4
0.6
0.8
1.0
VOLTS POLARIZATION

Figure 12

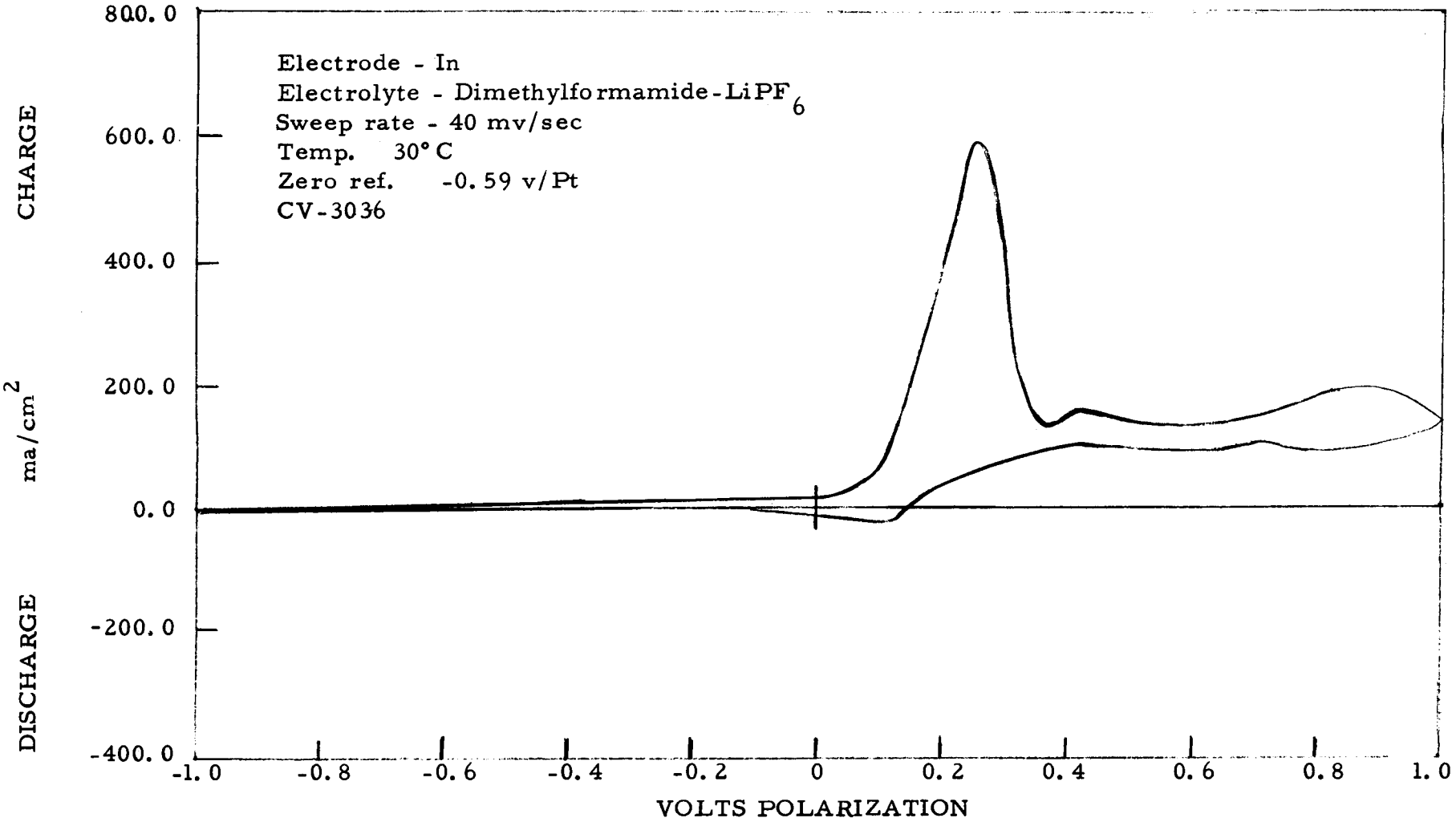
800.0
600.0
400.0
200.0
0.0
-200.0
-400.0
CHARGE
DISCHARGE
ma/cm 2
Electrode - In
Electrolyte - Dimethylformamide-LiPF6
Sweep rate - 40 mv/sec
Temp. 30° C
Zero ref. -0.59 v/Pt
CV-3036
-1.0
-0.8
-0.6
-0.4
-0.2
0
0.2
0.4
0.6
0.8
1.0
VOLTS POLARIZATION

Figure 13

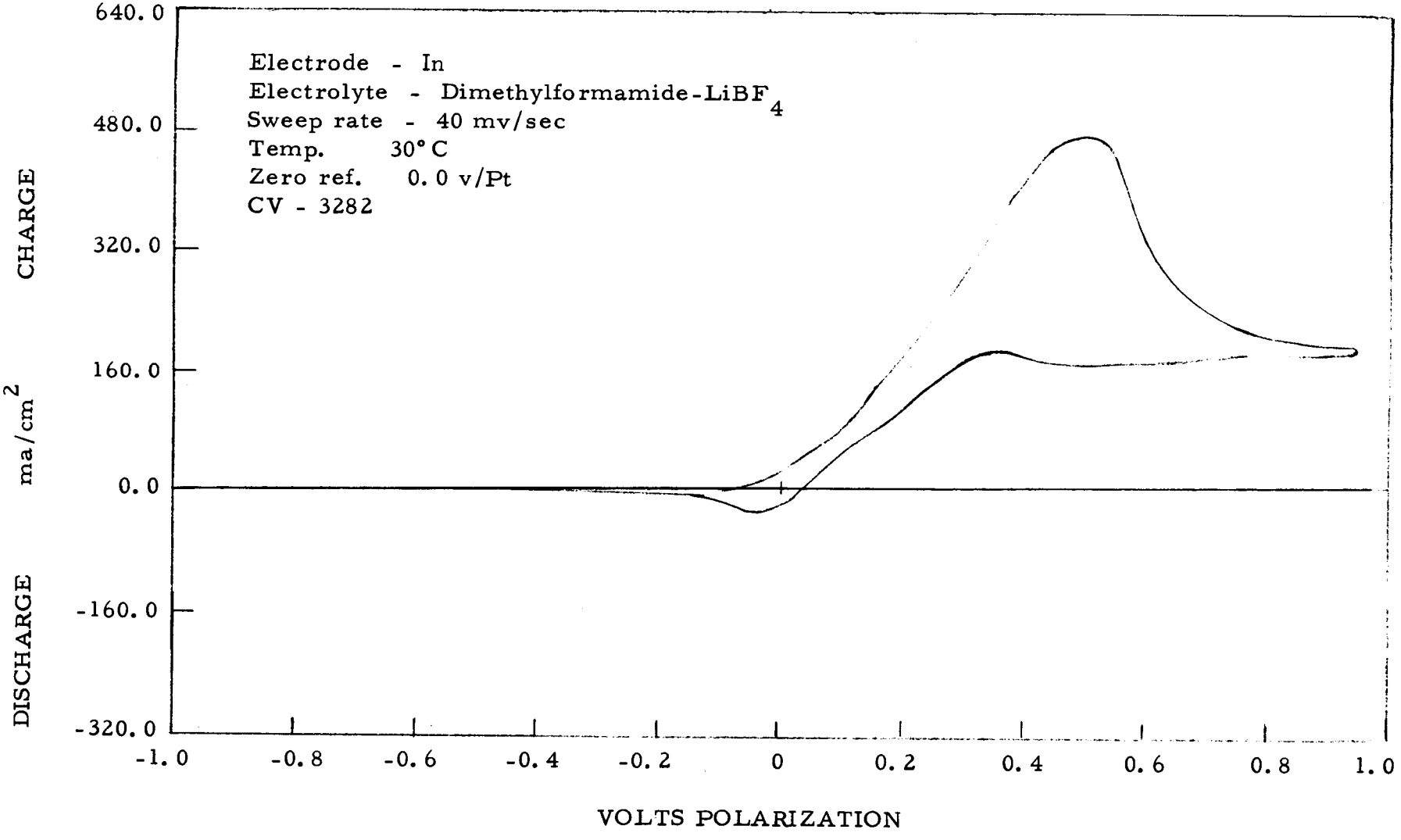
Electrode - In
Electrolyte - Dimethylformamide-LiBF4
Sweep rate - 40 mv/sec
Temp. 30° C
Zero ref. 0.0 v/Pt
CV - 3282
640.0
480.0
320.0
160.0
0.0
-160.0
-320.0
CHARGE
ma/cm2
DISCHARGE
-1.0
-0.8
-0.6
-0.4
-0.2
0
0.2
0.4
0.6
0.8
1.0
VOLTS POLARIZATION

Figure 14

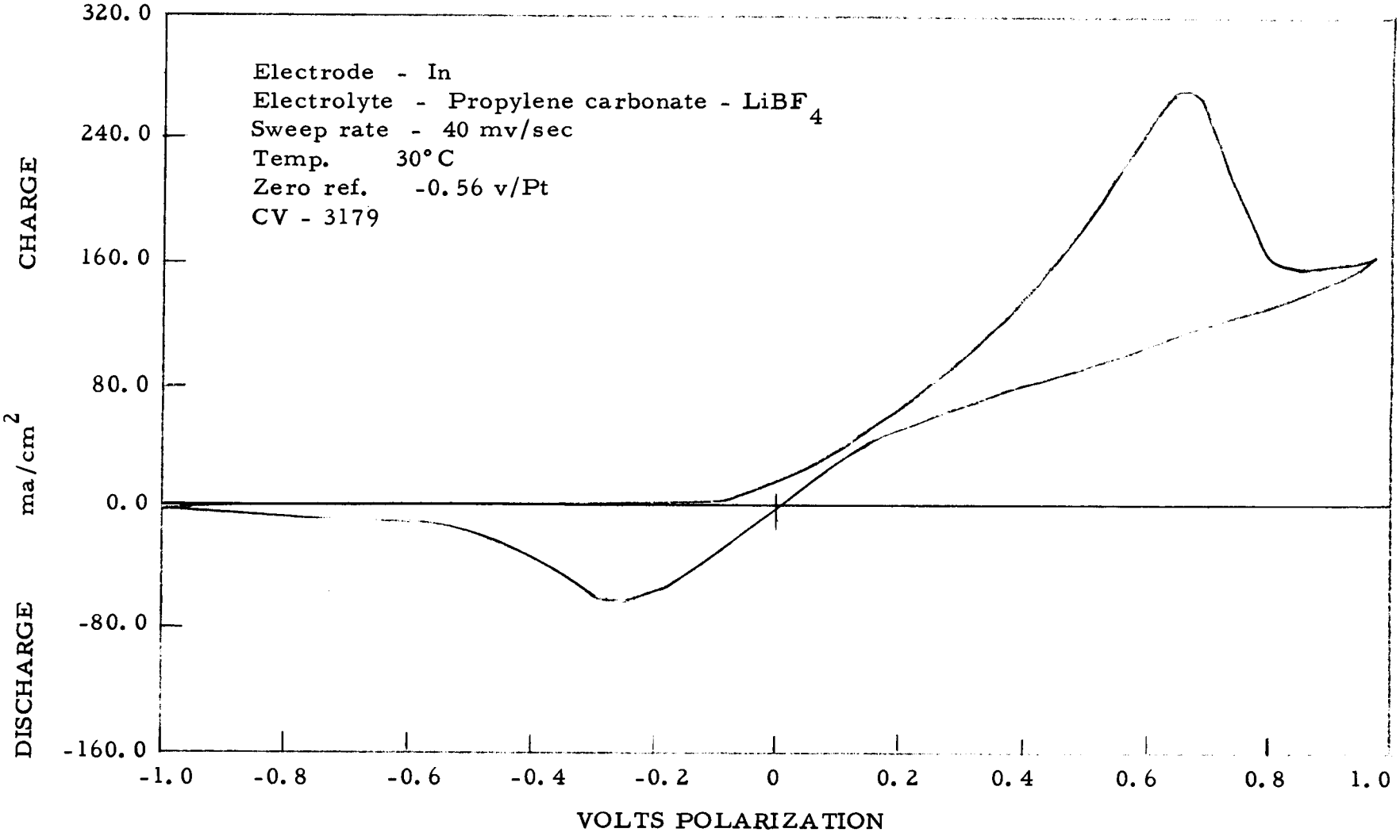
Electrode - In
Electrolyte - Propylene carbonate - $LiBF_4$
Sweep rate - 40 mv/sec
Temp. 30° C
Zero ref. -0.56 v/Pt
CV - 3179
320.0
240.0
160.0
80.0
0.0
-80.0
-160.0
CHARGE
DISCHARGE
ma/cm^2
-1.0
-0.8
-0.6
-0.4
-0.2
0
0.2
0.4
0.6
0.8
1.0
VOLTS POLARIZATION

Figure 15

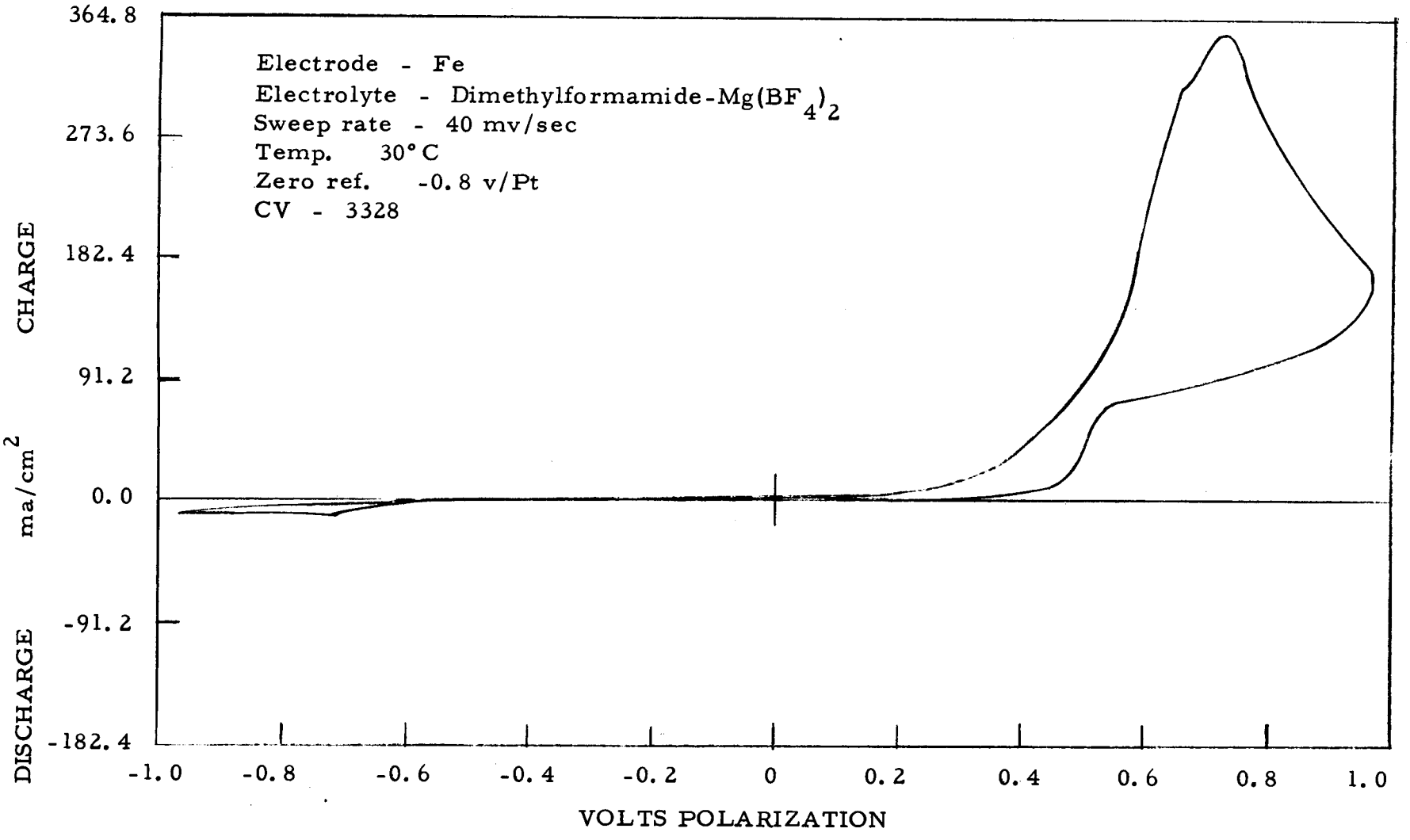
Electrode - Fe
Electrolyte - Dimethylformamide-Mg(BF4)2
Sweep rate - 40 mv/sec
Temp. 30° C
Zero ref. -0.8 v/Pt
CV - 3328
364.8
273.6
182.4
91.2
0.0
-91.2
-182.4
CHARGE
DISCHARGE
ma/cm2
-1.0
-0.8
-0.6
-0.4
-0.2
0
0.2
0.4
0.6
0.8
1.0
VOLTS POLARIZATION

Figure 16

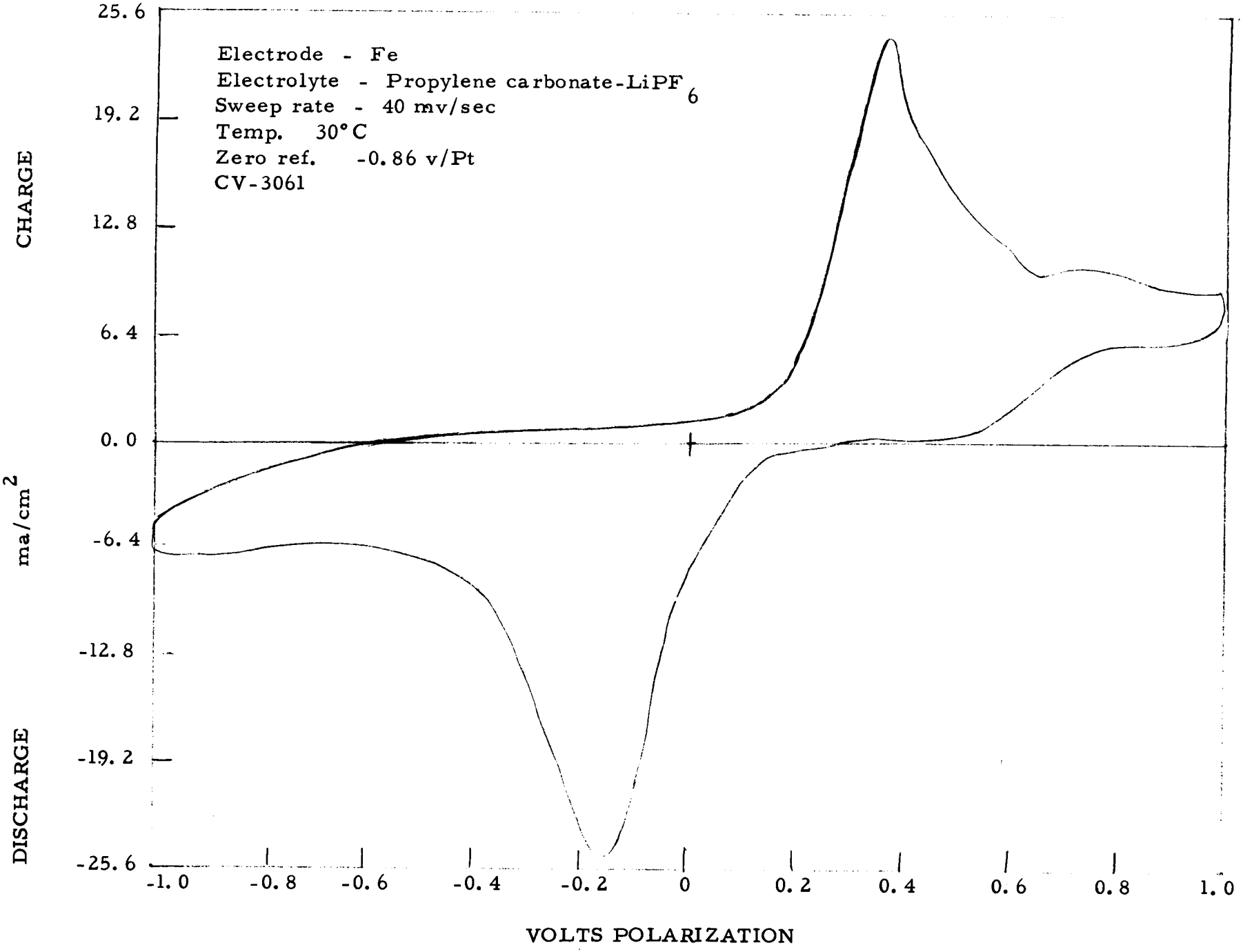
Electrode - Fe
Electrolyte - Propylene carbonate-LiPF6
Sweep rate - 40 mv/sec
Temp. 30°C
Zero ref. -0.86 v/Pt
CV-3061
CHARGE
DISCHARGE
ma/cm2
25.6
19.2
12.8
6.4
0.0
-6.4
-12.8
-19.2
-25.6
-1.0
-0.8
-0.6
-0.4
-0.2
0
0.2
0.4
0.6
0.8
1.0
VOLTS POLARIZATION

Figure 17

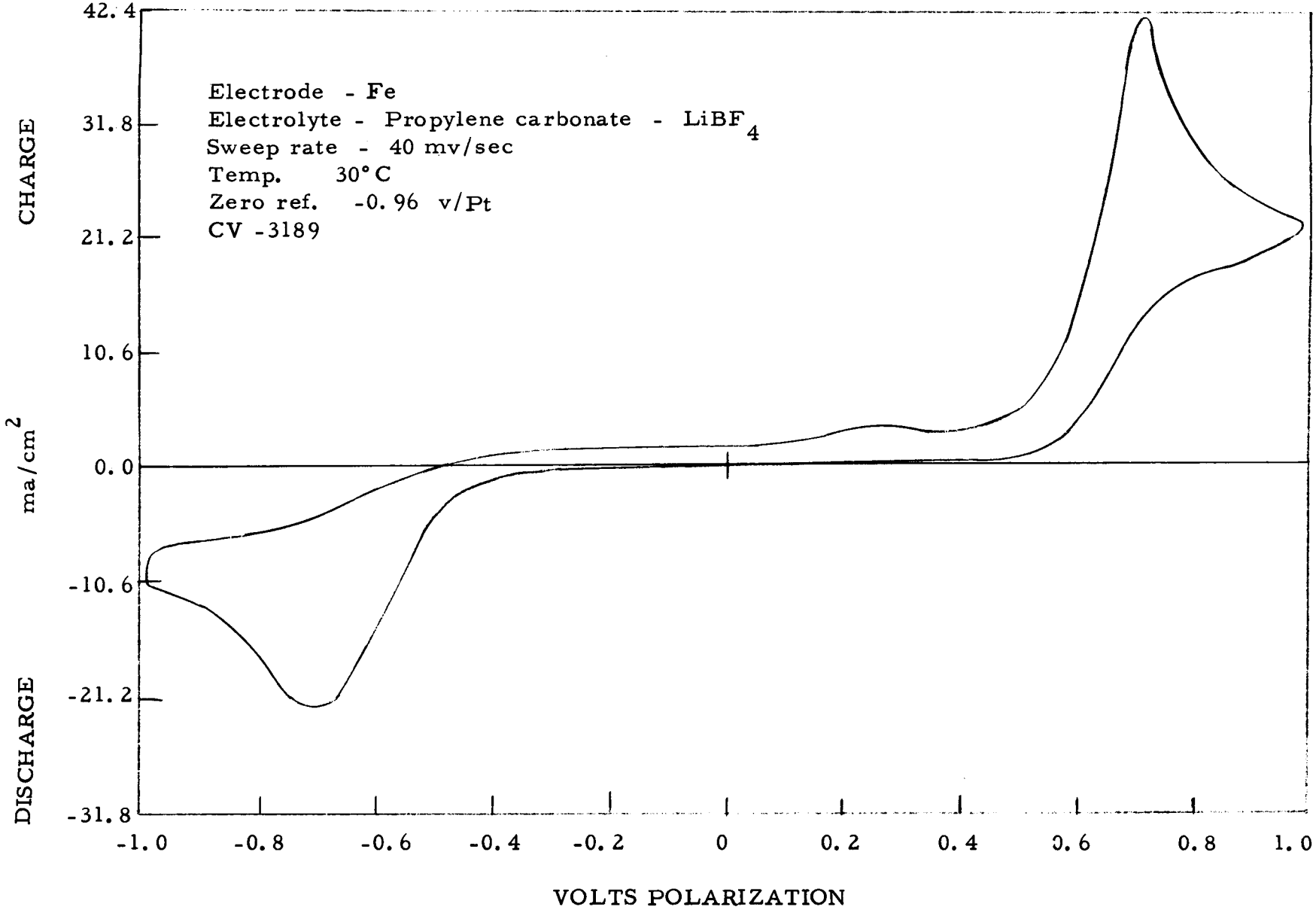
Electrode - Fe
Electrolyte - Propylene carbonate - $LiBF_4$
Sweep rate - 40 mv/sec
Temp. 30° C
Zero ref. -0.96 v/Pt
CV -3189
CHARGE
DISCHARGE
ma/cm^2
42.4
31.8
21.2
10.6
0.0
-10.6
-21.2
-31.8
-1.0
-0.8
-0.6
-0.4
-0.2
0
0.2
0.4
0.6
0.8
1.0
VOLTS POLARIZATION

Figure 18

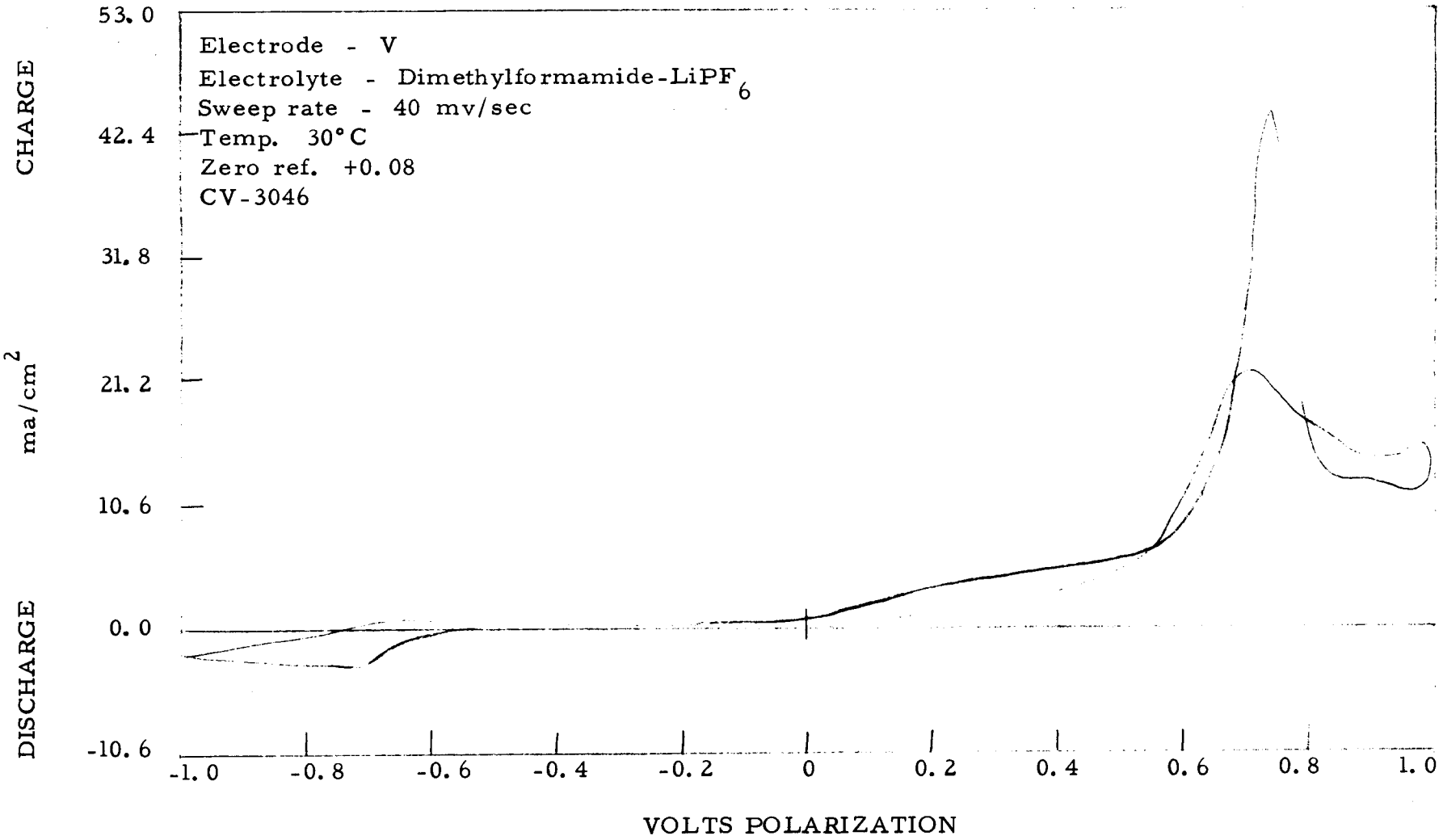
Electrode - V
Electrolyte - Dimethylformamide-LiPF6
Sweep rate - 40 mv/sec
Temp. 30°C
Zero ref. +0.08
CV-3046
CHARGE
DISCHARGE
ma/cm2
53.0
42.4
31.8
21.2
10.6
0.0
-10.6
-1.0
-0.8
-0.6
-0.4
-0.2
0
0.2
0.4
0.6
0.8
1.0
VOLTS POLARIZATION

Figure 19

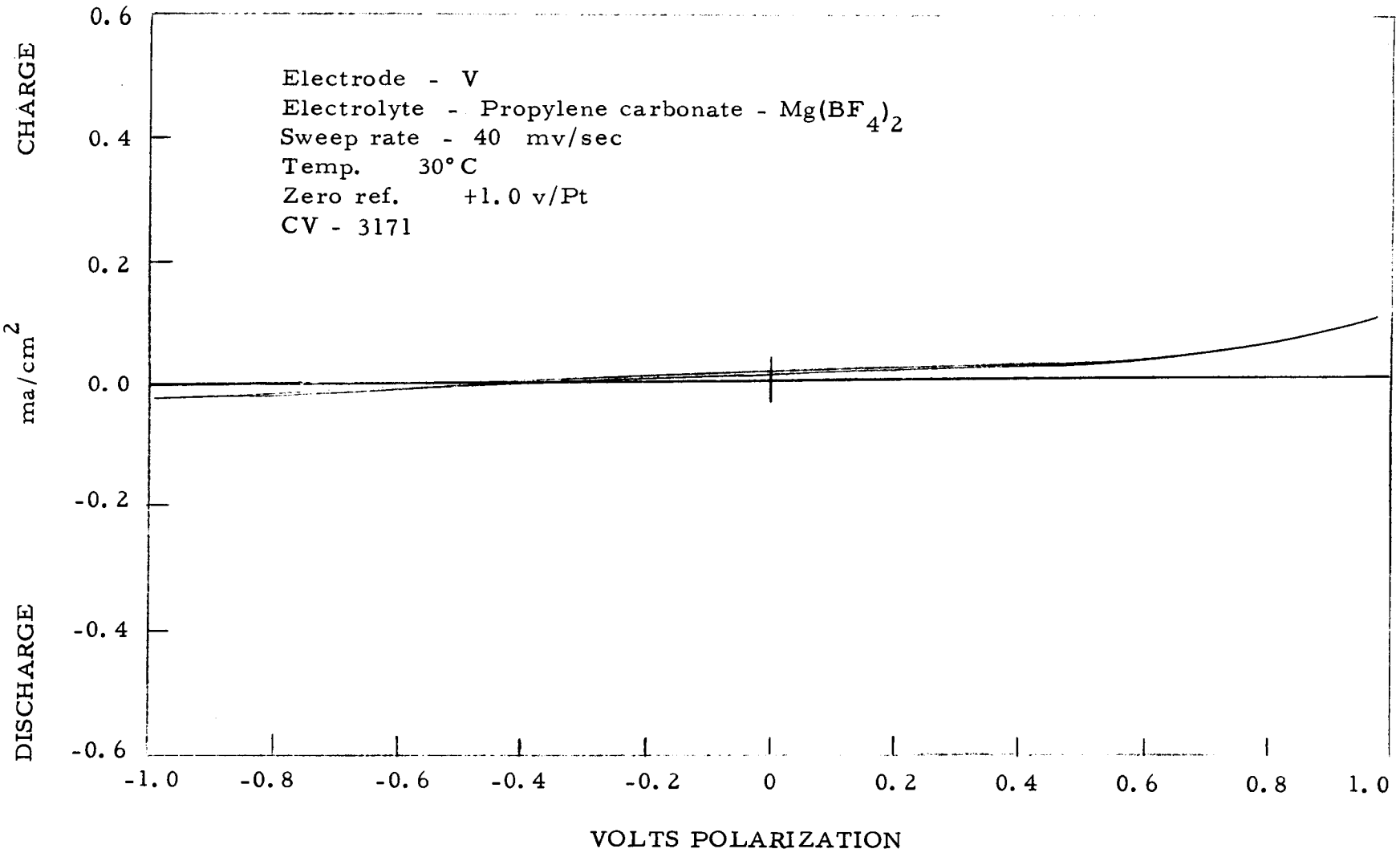
Electrode - V
Electrolyte - Propylene carbonate - $Mg(BF_4)_2$
Sweep rate - 40 mv/sec
Temp. 30° C
Zero ref. +1.0 v/Pt
CV - 3171
CHARGE
DISCHARGE
ma/cm^2
0.6
0.4
0.2
0.0
-0.2
-0.4
-0.6
-1.0
-0.8
-0.6
-0.4
-0.2
0
0.2
0.4
0.6
0.8
1.0
VOLTS POLARIZATION

Figure 20

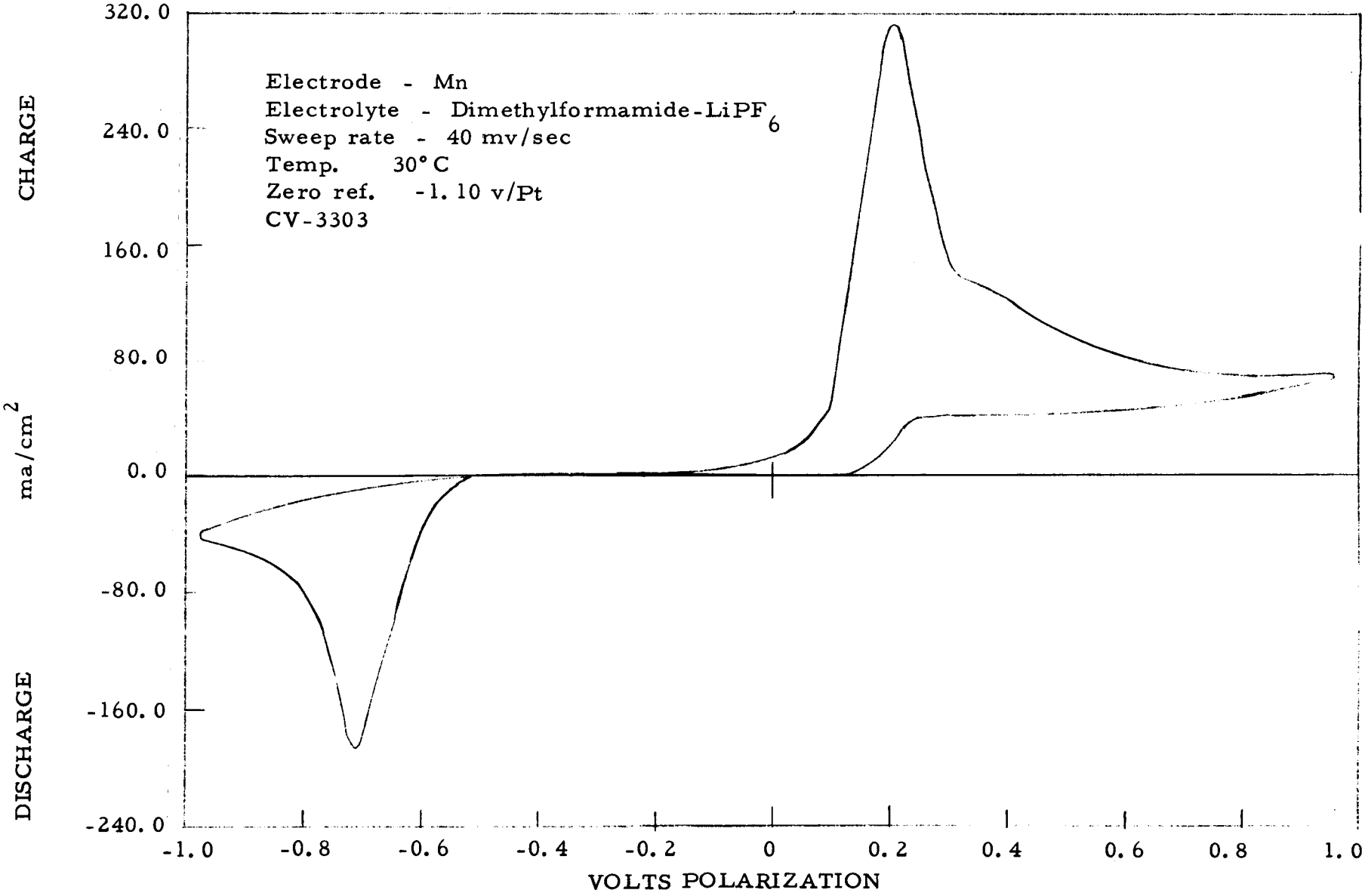
Electrode - Mn
Electrolyte - Dimethylformamide-LiPF6
Sweep rate - 40 mv/sec
Temp. 30° C
Zero ref. -1.10 v/Pt
CV-3303
CHARGE
DISCHARGE
ma/cm2
320.0
240.0
160.0
80.0
0.0
-80.0
-160.0
-240.0
-1.0
-0.8
-0.6
-0.4
-0.2
0
0.2
0.4
0.6
0.8
1.0
VOLTS POLARIZATION

Figure 21

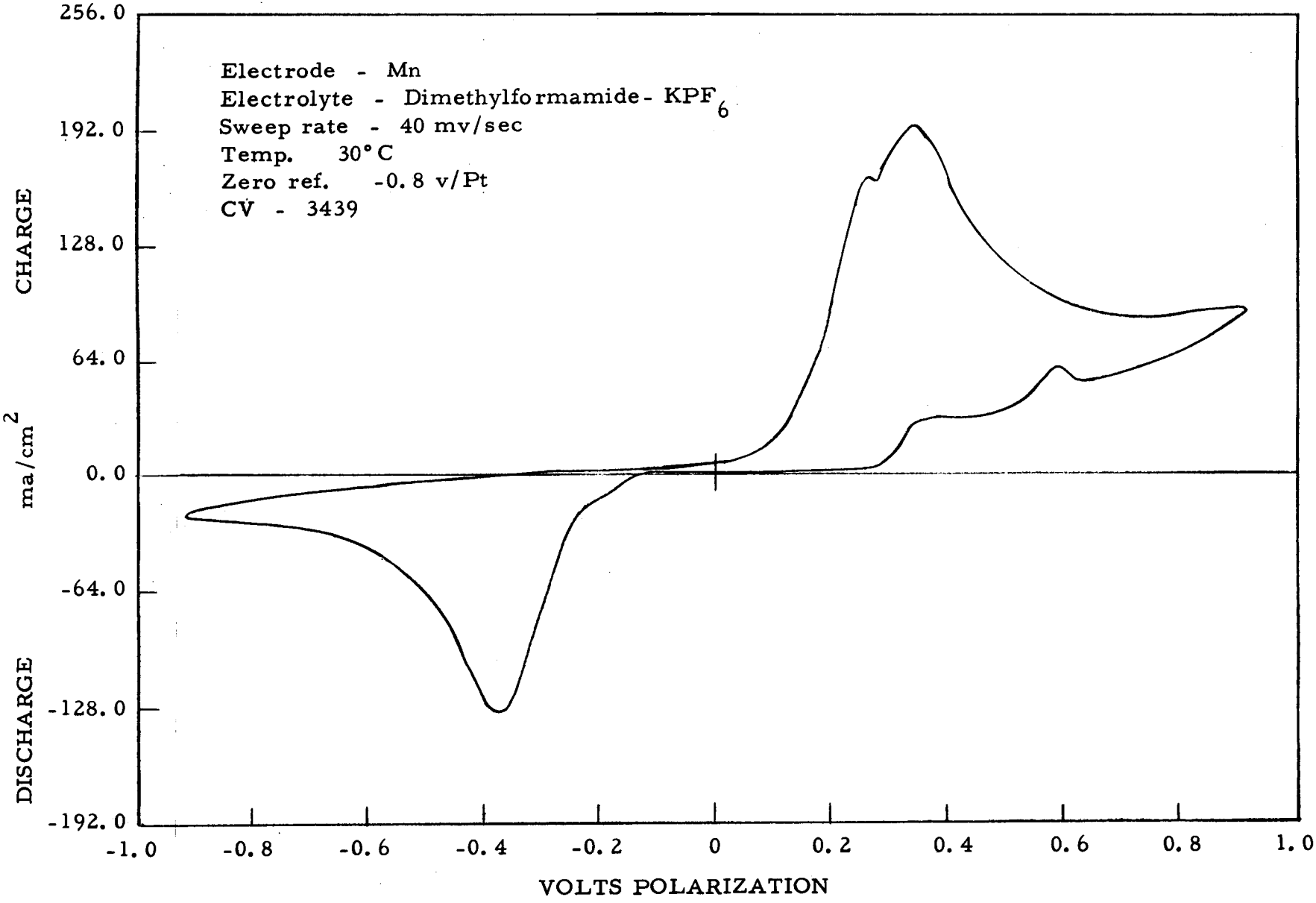
Electrode - Mn
Electrolyte - Dimethylformamide - KPF_6
Sweep rate - 40 mv/sec
Temp. 30° C
Zero ref. -0.8 v/Pt
CV - 3439
256.0
192.0
128.0
64.0
0.0
-64.0
-128.0
-192.0
CHARGE
DISCHARGE
ma/cm^2
-1.0
-0.8
-0.6
-0.4
-0.2
0
0.2
0.4
0.6
0.8
1.0
VOLTS POLARIZATION

Figure 22

B. TABLES OF CYCLIC VOLTAMMETRIC DATA

Included in this section are tables listing parameters derived from the cyclic voltammograms. These parameters are as follows:

1. Sweep index - This is a relative figure of merit taking into account peak height, sweep rate, and discharge capacity. This parameter is described in more detail in an earlier report (Ref. 2, p. 80).

2. Peak current density range - Relative magnitude of peak currents classified according to page 2.

3. ΔV_p - Peak-to-peak displacement in volts of charge and discharge reactions giving a measure of overall electrode reversibility, or in more practical terms, a measure of suitability of the electrochemical system for second battery application.

4. Coulombic ratio - Ratio of cathodic to anodic peak area. Values significantly in excess of unity for the pre-formed electrodes (chlorinated and fluorinated metals) are indicative of the contribution of the original cathodic material to the discharge reaction independent of the material formed by the preceding charge sweep.

5. Discharge capacity - Measure of discharge utilization per unit area of electrode surface, when compared with the coulombic ratio except for values of the latter greater than unity.

Also included are tables listing the systems causing voltage and current overload of the instrumentation preventing recordable voltammograms as well as those systems failing to exhibit either anodic or cathodic peaks. In cases of solutions having varying molality, the concentrations are included with the designated system. The concentration of all solutions are listed in Table I.

TABLE IV

SYSTEMS CAUSING VOLTAGE OVERLOAD
OF INSTRUMENTATION
CHLORIDE AND PERCHLORATE ELECTROLYTES

System	CV	Max. Anod. C. D. ma/cm^2	Max. Cath. C. D. ma/cm^2
$Zn/DMF-CaCl_2$	2958	400	100
$Zn/PC-CaCl_2$	3195	nil	nil
$Cd/PC-CaCl_2$	3196	nil	nil
$Mo/PC-MgCl_2$	2970	80	20
$Mo/PC-CaCl_2$	3198	40	nil
$Mo/PC-AlCl_3 + LiCl$	3366	2400	nil
$In/DMF-CaCl_2$	2978	200	nil
$In/PC-CaCl_2$	3197	nil	nil
$Fe/DMF-CaCl_2$	2969	200	20
$V/DMF-LiClO_4$	3316	2400	nil
$V/DMF-CaCl_2$	2977	1600	nil
$V/DMF-AlCl_3 + LiCl$	3393	2400	nil
$V/PC-AlCl_3 + LiCl$	3372	2400	nil
$Cr/DMF-LiCl$	3310	2400	nil
$Cr/DMF-LiClO_4$	3317	2800	nil
$Cr/DMF-AlCl_3 + LiCl$	3394	2800	nil
$Mn/PC-LiClO_4$	3414	400	4

DMF - Dimethylformamide

PC - Propylene carbonate

TABLE V

SYSTEMS CAUSING VOLTAGE OVERLOAD
OF INSTRUMENTATION
FLUORIDE ELECTROLYTES

System	CV	Max. Anod. C. D. ma/cm^2	Max. Cath. C. D. ma/cm^2
Zn/DMF-$Mg(PF_6)_2$	3089	400	600
Zn/DMF-PF_5	2985	1600	600
Zn/DMF-$Mg(BF_4)_2$	3323	1200	800
Zn/DMF-$Ca(BF_4)_2$	3353	1600	1600
Zn/DMF-BF_3	3265	1200	450
Zn/PC-$Mg(BF_4)_2$	3162	1200	800
Cd/DMF-$Mg(PF_6)_2$	3090	1600	1200
Cd/DMF-$Ca(PF_6)_2$	3078	1600	800
Cd/DMF-$Mg(BF_4)_2$	3324	1200	1200
Cd/DMF-$Ca(BF_4)_2$	3354	1600	1600
Cd/DMF-BF_3	3264	1200	450
Cd/PC-$Mg(PF_6)_2$	3135	1200	1200
Cd/PC-$Ca(PF_6)_2$	3153	400	300
Cd/PC-$LiBF_4$	3174	400	1200
Cd/PC-$Mg(BF_4)_2$	3163	1200	800
Cd/PC-$Ca(BF_4)_2$	3210	400	200
Mo/DMF-$Mg(PF_6)_2$	3091	1600	nil
Mo/DMF-$Ca(PF_6)_2$	3079	1200	100

DMF - Dimethylformamide

PC - Propylene carbonate

TABLE V (Cont'd.)

System	CV	Max. Anod. C. D. ma/cm^2	Max. Cath. C. D. ma/cm^2
Mo/DMF-$Mg(BF_4)_2$	3325	1600	nil
Mo/DMF-$Ca(BF_4)_2$	3355	1600	nil
Mo/DMF-BF_3	3263	1200	nil
Mo/PC-$Mg(PF_6)_2$	3136	800	nil
Mo/PC-$Ca(PF_6)_2$	3154	1200	nil
Mo/PC-$Mg(BF_4)_2$	3164	1200	nil
In/DMF-$Mg(PF_6)_2$	3092	1600	400
In/DMF-$Ca(PF_6)_2$	3080	1600	800
In/DMF-$Mg(BF_4)_2$	3326	1200	1200
In/DMF-$Ca(BF_4)_2$	3356	1600	1600
In/DMF-BF_3	3262	1200	800
In/PC-$Mg(PF_6)_2$	3142	800	480
In/PC-$Ca(PF_6)_2$	3155	1200	800
In/PC-$Mg(BF_4)_2$	3165	1200	1200
In/PC-$Ca(BF_4)_2$	3216	400	400
Fe/DMF-PF_5	2991	800	nil
Fe/DMF-BF_3	3261	1200	200
V/DMF-PF_5	2984	200	200

DMF - Dimethylformamide

PC - Propylene carbonate

TABLE V (Cont'd.)

System	CV	Max. Anod. C. D. ma/cm^2	Max. Cath. C. D. ma/cm^2
Cr/DMF-$Ca(PF_6)_2$	3336	800	nil
Cr/DMF-PF_5	3351	800	nil
Cr/DMF-$LiBF_4$	3289	1600	nil
Cr/DMF-$Mg(BF_4)_2$	3334	1600	nil
Cr/DMF-$Ca(BF_4)_2$	3364	1200	nil
Cr/DMF-BF_3	3266	1200	2
Cr/PC-PF_5	3349	800	nil
Cr/PC-$Ca(BF_4)_2$	3348	1200	nil
Mn/DMF-$Ca(PF_6)_2$	3088	1600	400
Mn/DMF-PF_5	3352	800	800
Mn/DMF-$Mg(BF_4)_2$	3335	1600	1600
Mn/DMF-$Ca(BF_4)_2$	3365	1200	1200
Mn/DMF-BF_3	3267	1200	400
Mn/PC-PF_5	3350	800	800
Mn/PC-$Ca(BF_4)_2$	3347	1200	1200

DMF - Dimethylformamide

PC - Propylene carbonate

TABLE VI

SYSTEMS CAUSING CURRENT OVERLOAD **
OF INSTRUMENTATION

System	CV	Max. Anod. C. D. ma/cm^2	Max. Cath. C. D. ma/cm^2
V/DMF-LiCl	3309	ov	nil

** ov-maximum current greater than 4.8 amp/cm^2

DMF - Dimethylformamide

TABLE VII

PEAK CURRENT DENSITY RANGE
CHLORIDE AND PERCHLORATE ELECTROLYTES

System	CV	Anodic	Cathodic
$Cd/DMF-CaCl_2$	2963	high	high
$Cd/PC-LiClO_4 + AlCl_3$	3236	medium high	medium high
$In/DMF-AlCl_3 + LiCl$	3392	high	medium high
$In/PC-LiClO_4$	3246	medium low	low
$In/PC-MgCl_2$	2971	high	high
$In/PC-AlCl_3 + LiCl$	3382	medium high	medium low
$Fe/PC-AlCl_3 + LiCl$	3371	medium low	low
Mn/DMF-LiCl	3315	low	low

DMF - Dimethylformamide

PC - Propylene carbonate

TABLE VIII

PEAK CURRENT DENSITY RANGE
FLUORIDE ELECTROLYTES

System	CV	Anodic	Cathodic
Zn/DMF-$Ca(PF_6)_2$	3077	high	high
Zn/DMF-$LiBF_4$	3272	high	medium high
Zn/DMF-$Mg(BF_4)_2$	3323	very high	very high
Zn/PC-$Mg(PF_6)_2$	3134	medium high	medium high
Zn/PC-$Ca(PF_6)_2$	3152	medium low	medium high
Zn/PC-$LiBF_4$	3173	medium low	medium low
Zn/PC-$Ca(BF_4)_2$	3209	medium low	medium low
Cd/DMF-PF_5	2990	very high	medium low
Cd/DMF-$LiBF_4$	3273	very high	very high
Mo/DMF-$LiPF_6$	3031	low	low
Mo/PC-$LiPF_6$	3051	medium high	low
In/DMF-$LiBF_4$	3282	very high	medium low
In/PC-$LiPF_6$	3056	high	medium high
In/PC-$LiBF_4$	3179	high	medium high
Fe/DMF-$Mg(PF_6)_2$	3041	very high	high
Fe/DMF-$Mg(PF_6)_2$	3094	medium high	high
Fe/DMF-$Ca(PF_6)_2$	3082	high	high
Fe/DMF-$Ca(BF_4)_2$	3358	very high	medium high
Fe/PC-$LiPF_6$	3061	medium low	medium low
Fe/PC-$LiBF_4$	3189	medium low	medium low
Fe/PC-$Mg(BF_4)_2$	3166	high	high
V/DMF-$LiPF_6$	3046	medium low	low
V/DMF-$Mg(PF_6)_2$	3099	medium low	low

DMF - Dimethylformamide

PC - Propylene carbonate

TABLE VIII (Cont'd.)

System	CV	Anodic	Cathodic
$V/DMF-Ca(PF_6)_2$	3087	medium low	low
$Mn/DMF-LiPF_6$	3072	high	medium high
$Mn/DMF-LiPF_6$	3303	high	high
$Mn/DMF-KPF_6$	3439	high	high
$Mn/DMF-LiBF_4$	3290	very high	medium high

DMF - Dimethylformamide

PC - Propylene carbonate

TABLE IX

SWEEP INDEX *

System	CV	Anodic $ohm^{-1}cm^{-2}$	Cathodic $ohm^{-1}cm^{-2}$
$Zn/PC\text{-}Mg(PF_6)_2$	3134	12.0	2.9
$Cd/DMF\text{-}LiBF_4$	3273	320.0	750.0
$Fe/PC\text{-}LiPF_6$	3061	2.4	3.2
$Mn/DMF\text{-}LiPF_6$	3072	-	14.1
$Mn/DMF\text{-}KPF_6$	3439	29.5	37.0

DMF - Dimethylformamide

PC - Propylene carbonate

$$* \frac{(\text{peak c.d.})^2 \times 100}{\text{sweep rate} \times \text{coul/cm}^2}$$

TABLE X

ΔV_p, COULOMBIC RATIO, AND DISCHARGE CAPACITY

System	CV	ΔV_p *	Coul. ** Ratio	Disch. Capac. coul/cm^2
Zn/DMF-$Ca(PF_6)_2$	3077	0.3	-	-
Zn/DMF-$LiBF_4$	3272	0.41	-	-
Zn/PC-$Mg(PF_6)_2$	3134	1.2	1.30	2.11
Zn/PC-$Ca(BF_4)_2$	3209	0.75	-	-
Cd/DMF-$CaCl_2$	2963	-	-	0.31
Cd/DMF-$LiBF_4$	3273	0.057	0.39	4.8
In/DMF-$LiBF_4$	3282	0.56	-	-
In/PC-$MgCl_2$	2971	-	0.25	0.73
In/PC-$LiPF_6$	3056	0.70	-	-
In/PC-$LiBF_4$	3179	0.9	-	-
Fe/PC-$LiPF_6$	3061	0.52	0.86	0.48
Fe/PC-$LiBF_4$	3189	1.4	-	-
Mn/DMF-$LiPF_6$	3072	1.0	0.27	1.37
Mn/DMF-$LiPF_6$	3303	0.9	-	-
Mn/DMF-KPF_6	3439	0.7	0.37	1.16
Mn/DMF-$LiBF_4$	3290	0.7	-	-

* Voltage separating anodic to cathodic peaks

** Ratio of cathodic to anodic peak areas

DMF - Dimethylformamide

PC - Propylene carbonate

TABLE XI

SYSTEMS EXHIBITING ANODIC PEAK ONLY*

System	CV	Peak Current Density Range
$Zn/PC-LiClO_4 + AlCl_3$	3231	medium low
$Mo/DMF-CaCl_2$	2968	very low
$Mo/DMF-PF_5$	2996	low (a)
$Mo/PC-LiClO_4 + AlCl_3$	3241	medium high
$In/DMF-LiPF_6$	3036	very high (a)
$In/PC-LiCl + LiClO_4$	3119	low
$Fe/DMF-LiBF_4$	3284	medium high
$Fe/DMF-Mg(BF_4)_2$	3328	very high (b)
$Fe/PC-LiClO_4 + AlCl_3$	3251	low (a)
$Fe/PC-MgCl_2$	2976	medium low (a)
$Fe/PC-Mg(PF_6)_2$	3141	low
$Fe/PC-Ca(PF_6)_2$	3156	medium low (b)
$V/DMF-Mg(ClO_4)_2$	3444	high (a)
$V/DMF-KPF_6$	3429	medium low
$V/DMF-Mg(BF_4)_2$	3333	very low
$V/PC-LiClO_4$	3408	medium high
$V/PC-LiClO_4 + AlCl_3$	3256	high
$V/PC-CaCl_2$	3202	very low

* Maximum cathodic current density in very low range (<1 ma/cm^2) unless otherwise noted.

(a) Low range cathodic (<10 ma/cm^2)

(b) Medium low range cathodic (10-50 ma/cm^2)

DMF - Dimethylformamide

PC - Propylene carbonate

TABLE XI (Cont'd.)

System	CV	Peak Current Density Range
$Cr/DMF-Mg(ClO_4)_2$	3449	high
$Cr/DMF-LiPF_6$	3308	medium low
$Cr/PC-LiClO_4$	3413	low
$Cr/PC-AlCl_3 + LiCl$	3377	medium high (a)
$Mn/DMF-LiClO_4$	3322	high
$Mn/DMF-AlCl_3 + LiCl$	3399	high
$Mn/PC-AlCl_3 + LiCl$	3387	medium low
$Mn/PC-Ca(PF_6)_2$	3346	low

* Maximum cathodic current density in very low range (<1 ma/cm^2) unless otherwise noted.

(a) Low range cathodic (<10 ma/cm^2)

(b) Medium low range cathodic (10-50 ma/cm^2)

DMF - Dimethylformamide

PC - Propylene carbonate

TABLE XII

SYSTEMS EXHIBITING CATHODIC PEAK ONLY

System	CV	Peak Current Density Range
Fe/PC-$Ca(BF_4)_2$	3221	medium low (a)

(a) Maximum anodic current density in medium high range (50-100 ma/cm^2)

PC - Propylene carbonate

TABLE XIII

SYSTEMS EXHIBITING NO PEAKS *

System	CV
Zn/PC-LiCl + $LiClO_4$	3104 (d)
Zn/PC-PF_5	3001 (c)
Cd/PC-LiCl + $LiClO_4$	3109 (d)
Cd/PC-PF_5	3006 (b)
Mo/DMF-$LiBF_4$	3278 (b)
Mo/PC-LiCl + $LiClO_4$	3114 (d)
Mo/PC-PF_5	3011 (c)
Mo/PC-$LiBF_4$	3184 (b)
Mo/PC-$Ca(BF_4)_2$	3215 (c)
In/DMF-PF_5	2983 (a)
In/PC-PF_5	3016 (c)
Fe/PC-LiCl + $LiClO_4$	3124
Fe/PC-$CaCl_2$	3199
Fe/PC-PF_5	3021 (d)
V/DMF-$LiBF_4$	3294 (d)
V/DMF-$Ca(BF_4)_2$	3359 (d)
V/DMF-BF_3	3257

* Maximum current density in very low range (<1 ma/cm^2) unless otherwise noted.

(a) High range (100-300 ma/cm^2)

(b) Medium high range (50-100 ma/cm^2)

(c) Medium low range (10-50 ma/cm^2)

(d) Low range (1-10 ma/cm^2)

DMF - Dimethylformamide

PC - Propylene carbonate

TABLE XIII (Cont'd.)

System	CV
V/PC-LiCl + $LiClO_4$	3129
V/PC-$LiPF_6$	3066
V/PC-KPF_6	3402 (d)
V/PC-$Mg(PF_6)_2$	3147
V/PC-$Ca(PF_6)_2$	3161
V/PC-PF_5	3026
V/PC-$LiBF_4$	3194
V/PC-$Mg(BF_4)_2$	3171
V/PC-$Ca(BF_4)_2$	3226
Cr/DMF-KPF_6	3434 (d)
Cr/PC-KPF_6	3419 (d)
Cr/PC-$Ca(PF_6)_2$	3341
Mn/DMF-$Mg(ClO_4)_2$	3454
Mn/PC-KPF_6	3424 (a)

* Maximum current density in very low range (1 ma/cm^2) unless otherwise noted.

(a) High range (100-300 ma/cm^2)

(b) Medium high range (50-100 ma/cm^2)

(c) Medium low range (10-50 ma/cm^2)

(d) Low range (1-10 ma/cm^2)

DMF - Dimethylformamide

PC - Propylene carbonate

II. REFERENCES

1. Whittaker Corporation, Narmco Research and Development Division, Fifth Quarterly Report, NASA Contract NAS 3-8509, NASA Report CR-72293, August 1967.

2. Whittaker Corporation, Narmco Research and Development Division, First Quarterly Report, NASA Contract NAS 3-8509, NASA Report CR-72069, August 1966.

DISTRIBUTION LIST

National Aeronautics and Space Admin.
Washington, D. C. 20546
Attn: E. M. Cohn/RNW
A. M. Greg Andrus/PC

National Aeronautics and Space Admin.
Goddard Space Flight Center
Greenbelt, Maryland 20771
Attn: T. Hennigan, Code 716.2
J. Sherfey, Code 735
P. Donnelly, Code 636.2
E. R. Stroup, Code 636.2

National Aeronautics and Space Admin.
Langley Research Center
Instrument Research Division
Hampton, Virginia 23365
Attn: J. L. Patterson, MS 234
M. B. Seyffert, MS 112

National Aeronautics and Space Admin.
Langley Research Center
Hampton, Virginia 23365
Attn: S. T. Peterson
Harry Ricker

National Aeronautics and Space Admin.
Lewis Research Center
2100 Brookpark Road
Cleveland, Ohio 44135
Attn: Library, MS 60-3
N. D. Sanders, MS 302-1
John E. Dilley, MS 500-309
B. Lubarsky, MS 500-201
H, J. Schwartz, MS 500-201
R. B. King, MS 500-202 (2cys.)
V. F. Hlavin, MS 3-14 (Final only)
M. J. Saari, MS-500-202
J. J. Weber, MS 3-19
Report Control, MS 5-5
Dr. J. S. Fordyce, MS 6-1

National Aeronautics and Space Admin.
Scientific and Tech. Information Facility
P. O. Box 33
College Park, Maryland 20740
Attn: Acquisitions Branch (SQT-34054)
(2 cys. + 1 repro.)

National Aeronautics and Space Admin.
George C. Marshall Space Flight Center
Huntsville, Alabama 35812
Attn: Philip Youngblood
R. Boehme, Bldg. 4487.BB,
M-ASTR-EC

National Aeronautics and Space Admin.
Manned Spacecraft Center
Houston, Texas 77058
Attn: W. R. Dusenbury, Propulsion
and Energy Systems
R. Cohen, Gemini Project Office
R. Ferguson (EP-5)
J. T. Kennedy (EE-5)
F. E. Eastman (EE-4)

National Aeronautics and Space Admin.
Ames Research Center
Pioneer Project
Moffett Field, California 94035
Attn: J. R. Swain
A. S. Hertzog
J. Rubenzer, Biosatellite Project

Jet Propulsion Laboratory
4800 Oak Grove Drive
Pasadena, California 91103
Attn: A. Uchiyama

U. S. Army Engineer R and D Labs.
Fort Belvoir, Virginia 22060
Attn: Electrical Power Branch
SMOFB-EP

Commanding Officer
U. S. Army Electronics R and D Labs.
Fort Monmouth, New Jersey 07703
Attn: Power Sources Div., Code SELRA/PS

Research Office
R and D Directorate
Army Weapons Command
Rock Island, Illinois 61201
Attn: G. Riensmith, Chief

U. S. Army Research Office
Box CM, Duke Station
Durham, North Carolina 27706
Attn: Dr. W. Jorgensen

U. S. Army Research Office
Chief, R and D
Department of the Army
3 D 442, The Pentagon
Washington, D. C. 20546

Harry Diamond Laboratories
Room 300, Bldg. 92
Conn. Ave and Van Ness St., NW
Washington, D. C. 20438
Attn: N. Kaplan

Army Materiel Command
Research Division
AMCRD-RSCM-T-7
Washington, D. C. 20315
Attn: J. W. Crellin

Army Materiel Command
Development Division
AMCRO-DE-MO-P
Washington, D. C. 20315
Attn: M. D. Aiken

U. S. Army TRECOM
Fort Eustis, Virginia 23604
Attn: Dr. R. L. Echols (SMOFE-PSG)
L. M. Bartone (SMOFE-ASE)

U. S. Army Mobility Command
Research Division
Watten, Michigan 48090
Attn: O. Renius (AMSMO-RR)

U. S. Army R and L Liaison Group
(9851 DV) APO 757
New York, New York 10004
Attn: B. R. Stein

Office of Naval Research
Department of the Navy
Washington, D. C. 20360
Attn: Head, Power Branch, Code 429
H. W. Fox, Code 425

Naval Research Laboratory
Washington, D. C. 20390
Attn: Dr. J. C. White, Code 6160

U. S. Navy
Marine Engineering Laboratory
Annapolis, Maryland 21402
Attn: J. H. Harrison

Bureau of Naval Weapons
Department of the Navy
Washington, D. C. 20360
Attn: W. T. Beatson, Code RAAE-52
M. Knight, Code RAAE-50

Naval Ammunition Depot
Crane, Indiana 47522
Attn: E. Bruess
H. Schultz

Naval Ordnance Laboratory
Department of the Navy
Corona, California 91720
Attn: W. C. Spindler, Code 441

Army Reactors, DRD
U. S. Atomic Energy Commission
Washington, D. C. 20545
Attn: D. B. Hoatson

Naval Ordnance Laboratory
Department of the Navy
Silver Springs, Maryland 20900
Attn: P. B. Cole, Code WB

Bureau of Ships
Department of the Navy
Washington, D. C. 20360
Attn: B. B. Rosenbaum, Code 340
C. F. Viglotti, Code 660

Space Systems Division
Los Angeles AF Station
Los Angeles, California 90045
Attn: SSSD

Air Force Cambridge Research Lab. (CRFE)
L. G. Hanscom Field
Bedford, Massachusetts 01731
Attn: Dr. Richard Payne

Flight Vehicle Power Branch
Aero Propulsion Laboratory
Wright-Patterson AFB, Ohio 45433
Attn: J. E. Cooper

Headquarters, USAF (AFRDR-AS)
Washington, D. C. 20546
Attn: Maj. G. Starkey
Lt. Col. W. G. Alexander

Rome Air Development Center, ESD
Griffis AF Base, New York 13442
Attn: F. J. Mollura (RASSM)

National Bureau of Standards
Washington, D. C. 20234
Attn: Dr. W. J. Hamer

Office DDR and E, USE and BSS
The Pentagon
Washington, D. C. 20310
Attn: G. B. Wareham

Institute for Defense Analyses
R and E Support Division
400 Army-Navy Drive
Arlington, Virginia 22022
Att: R. Hamilton
Dr. G. C. Szego

U. S. Atomic Energy Commission
Auxiliary Power Branch (SNAP)
Division of Reactor Development
Washington, D. C. 20545
Attn: Lt. Col. G. H. Ogburn, Jr.

U. S. Atomic Energy Commission
Advanced Space Reactor Branch
Division of Reactor Development
Washington, D. C. 20545
Attn: Lt. Col. J. H. Anderson

Office of Technical Services
Department of Commerce
Washington, D. C. 20009

Aerojet-General Corporation
Von Karman Center
Building 312/Dept. 3111
Azusa, California 91703

Aeronutronic Division
Philco Corporation
Ford Road
Newport Beach, California 92660

Aerospace Corporation
P. O. Box 95085
Los Angeles, California 90045
Attn: Library

Burgess Battery Company
Foot of Exchange Street
Freeport, Illinois 61032
Attn: Dr. Howard J. Strauss

Aerospace Corporation
Systems Design Division
2350 East El Segundo Boulevard
El Segundo, California 90246
Attn: John G. Krisilas

Allis-Chalmers Manufacturing Company
1100 South 70th Street
Milwaukee, Wisconsin 53201
Attn: Dr. P. Joyner

American University
Massachusetts and Nebraska Avenues NW
Washington, D. C. 20016
Attn: Dr. R. T. Foley, Chemistry Dept.

Arthur D. Little, Incorporated
Acorn Park
Cambridge, Massachusetts 02140
Attn: Dr. Ellery W. Stone

Atomics International Division
North American Aviation, Incorporated
8900 DeSoto Avenue
Canoga Park, California 91304
Attn: Dr. H. L. Recht

Battelle Memorial Institute
505 King Avenue
Columbus, Ohio 43201
Attn: Dr. C. L. Faust

Bell Laboratories
Murray Hill, New Jersey 07971
Attn: U. B. Thomas

The Boeing Company
P. O. Box 3707
Seattle, Washington 98124

Borden Chemical Company
Central Research Laboratory
P. O. Box 9524
Philadelphia, Pennsylvania 19124

C and D Batteries
Division of Electric Autolite Company
Conshohocken, Pennsylvania 19428
Attn: Dr. Eugene Willihnganz

Calvin College
Grand Rapids, Michigan 49506
Attn: Prof. T. P. Dirkse

Catalyst Research Corporation
6101 Falls Road
Baltimore, Maryland 21209
Attn: J. P. Wooley

ChemCell, Incorporated
3 Central Avenue
East Newark, New Jersey 07029
Attn: Peter D. Richman

Delco Remy Division
General Motors Corporation
2401 Columbus Avenue
Anderson, Indiana 46011
Attn: Dr. J. J. Lander

Douglas Aircraft Company, Incorporated
Astropower Laboratory
2121 Campus Drive
Newport Beach, California 92663

Dynatech Corporation
17 Tudor Street
Cambridge, Massachusetts 02138
Attn: R. L. Wentworth

Eagle-Pitcher Company
P. O. Box 47
Joplin, Missouri 64802
Attn: E. M. Morse

General Electric Company
Battery Products Section
P. O. Box 114
Gainesville, Florida 32601
Attn: Dr. R. L. Hadley

Elgin National Watch Company
107 National Street
Elgin, Illinois 60120
Attn: T. Boswell

Electric Storage Battery Company
Missile Battery Division
2510 Louisburg Road
Raleigh, North Carolina 27604
Attn: A. Chreitzberg

Electric Storage Battery Company
Carl F. Norberg Research Center
Wardley, Pennsylvania 19068
Attn: Dr. R. A. Schaefer

Electrochimica Corporation
1140 O'Brien Drive
Menlo Park, California 94025
Attn: Dr. Morris Eisenberg

Electro-Optical Systems, Incorporated
300 North Halstead
Pasadena, California 91107
Attn: E. Findl

Emhart Manufacturing Company
Box 1620
Hartford, Connecticut 06101
Attn: Dr. W. P. Cadogan

Englehard Industries, Incorporated
497 Delancy Street
Newark, New Jersey 07105
Attn: Dr. J. G. Cohn

Dr. Arthur Fleischer
466 South Center Street
Orange, New Jersey 07050

Grumman Aircraft
CPGS Plant 35
Beth Page, Long Island, New York 11101
Attn: Bruce Clark

General Electric Company
Research and Development Center
Schenectady, New York 12301
Attn: Dr. H. Liebhafsky
Dr. R. C. Osthoff, Bldg. 37,

General Motors-Defense Research Labs.
6767 Hollister Street
Santa Barbara, California 93105
Attn: Dr. J. S. Smatko
Dr. C. R. Russell

General Telephone and Electronics Labs.
Baysi de, New York 11352
Attn: Dr. Paul Goldberg

Globe-Union, Incorporated
900 East Keefe Avenue
Milwaukee, Wisconsin 53201
Attn: Dr. Warren Towle

Gould-National Batteries, Incorporated
Engineering and Research Center
2630 University Avenue, SE
Minneapolis, Minnesota 55418
Attn: D. L. Douglas

Gulton Industries
Alkaline Battery Division
212 Durham Avenue
Metuchen, New Jersey 08840
Attn: Dr. Robert Shair

Leesona Moos Laboratories
Lake Success Park, Community Drive
Great Neck, New York 11021
Attn: Dr. H. Oswin

Livingston Electronic Corporation
Route 309
Montgomeryville, Pennsylvania 18936
Attn: William F. Meyers

Hughes Aircraft Corporation
Centinela Avenue and Teale Street
Culver City, California 90230
Attn: T. V. Carvey

Hughes Aircraft Corporation
Building 366, MS 524
El Segundo, California 90245
Attn: R. B. Robinson

Hughes Research Labs. Corp.
2011 Malibu Canyon Road
Malibu, California 90265
Attn: T. M. Hahn

ITT Federal Laboratories
500 Washington Avenue
Nutley, New Jersey 07110
Attn: Dr. P. E. Lightly

IIT Research Institute
10 West 35 Street
Chicago, Illinois 60616
Attn: Dr. H. T. Francis

Idaho State University
Department of Chemistry
Pocatello, Idaho 83201
Attn: Dr. G. Myron Arcand

Institute of Gas Technology
State and 34 Street
Chicago, Illinois 60616
Attn: B. S. Baker

John Hopkins University
Applied Physics Laboratory
8621 Georgia Avenue
Silver Springs, Maryland 20910

Lockheed Missiles and Space Co.,
3251 Hanover Street
Palo Alto, California 94304
Attn: Library
Dr. G. B. Adams

Lockheed Missiles and Space Co.
Department 52-30
Palo Alto, California 94304
Attn: J. E. Chilton

Lockheed Missiles and Space Co.
Department 65-82
Palo Alto, California 94304
Attn: Larry E. Nelson

Magna Corporation
Division of TRW, Inc.
101 South East Avenue
Anaheim, California
Attn: Dr. G. Rohrback

P. R. Mallory and Co., Inc.
Technical Services Laboratory
Indianapolis, Indiana 46206
Attn: A. S. Doty

P. R. Mallory and Co., Inc.
3029 East Washington Street
Indianapolis, Indiana 46206
Attn: Library

Marquardt Corporation
16555 Saticoy Street
Van Nuys, California 91406
Attn: Dr. H. G. Krull

Philco Corporation
Division of Ford Motor Company
Blue Bell, Pennsylvania 19422
Attn: Dr. Phillip Cholet

Radiation Applications, Inc.,
36-40 37th Street
Long Island City, New York 11101

Material Research Corporation
Orangeburg, New York 10962
Attn: V. E. Adler

Melpar
Technical Information Center
3000 Arlington Boulevard
Falls Church, Virginia 22046

Metals and Control Division
Texas Instruments, Inc.
34 Forest Street
Attleboro, Massachusetts 02703
Attn: Dr. E. M. Jost

Midwest Research Institute
425 Volker Boulevard
Kansas City, Missouri 64110
Attn: Dr. B. W. Beadle

Monsanto Research Corporation
Everett, Massachusetts 02149
Attn: Dr. J. O. Smith

North American Aviation, Inc.
Rocketdyne Division
6633 Canoga Avenue
Canoga Park, California 91303
Attn: Library

North American Aviation, Inc.
2214 Lakewood Boulevard
Downey, California 90241
Attn: Burden M. Otzinger

Ozark Mahoning Company
1870 S. Boulder Avenue
Tulso, Oklahoma 74119
Attn: Dr. James Beal

Power Information Center
University of Pennsylvania
3401 Market Street, Room 2107
Philadelphia, Pennsylvania 19104

Tyco Laboratories, Inc.
Bear Hill
Hickory Drive
Waltham, Massachusetts 02154
Attn: W. W. Burnett

Radio Corporation of America
Astro Division
Highstown, New Jersey 08520
Attn: Seymour Winkler

Radio Corporation of America
P. O. Box 800
Princeton, New Jersey 08540
Attn: L. Schulman

Sandia Corporation
Box 5800
Albuquerque, New Mexico 87115
Attn: Technical Library (2 copies)

Sonotone Corporation
Saw Mill River Road
Elmsford, New York 10523
Attn: A. Mundel

Texas Instruments, Inc.
13500 North Central Expressway
Dallas, Texas 75222
Attn: Dr. Isaac Trachtenberg

Thomas A. Edison Research Lab.
McGraw Edison Company
Watchung Avenue
West Orange, New Jersey 07052
Attn: Dr. P. F. Grieger

TRW Incorporated
TRW Systems Group
One Space Park
Redondo Beach, California 90278
Attn: Dr. A. Krausz, Bldg. 60, Rm 1470

TRW Incorporated
23555 Euclid Aven ue
Cleveland, Ohio 44117
Attn: Librarian

Union Carbide Corporation
Development Laboratory Library
P. O. Box 6056
Cleveland, Ohio 44101

Union Carbide Corporation
Parma Research Center
P. O. Box 6116
Cleveland, Ohio 44101
Attn: Library

University of California
Space Science Laboratory
Berkeley, California 94720
Attn: Dr. C. W. Tobias

University of Pennsylvania
Electrochemistry Laboratory
Philadelphia, Pennsylvania 19104
Attn: Prof. J. O'M Brockris

University of Toledo
Toledo, Ohio 43606
Attn: Dr. Albertine Krohn

Western Electric Company
Suite 802, RCA Building
Washington, D. C. 20006
Attn: R. T. Fiske

Westinghouse Electric Corporation
Research and Development Center
Churchill Borough
Pittsburgh, Pennsylvania 15235
Attn: Dr. A. Langer

Whittaker Corporation
Power Sources Division
3850 Olive Street
Denver, Colorado 80237
Attn: J. W. Reiter

Whittaker Corporation
Narmco R and D Division
12032 Vose Street
North Hollywood, California 91605
Attn: Dr. M. Shaw

Yardney Electric Corporation
40-50 Leonard Street
New York, New York 10013
Attn: Dr. George Dalin